https://doi.org/10.5194/cp-2020-20
Preprint. Discussion started: 27 February 2020

Climate of the Past Discussions

Holocene vegetation dynamics in response to climate change and hydrological processes in the Bohai region

Chen Jinxia[a,b,*], Shi Xuefa[a,b,*], Liu Yanguang[a,b], Qiao Shuqing[a,b], Yang Shixiong[c,d], Yan Shijuan[a,b], Lv Huahua[a,b], Li Xiaoyan[a,b], Li Chaoxin[a,b]

[a] Key Laboratory of Marine Sedimentology and Environmental Geology, First Institute of Oceanography, SOA, Qingdao 266061, China

[b] Laboratory for Marine Geology, Qingdao National Laboratory for Marine Science and Technology, Qingdao 266061, China

[c] Key Laboratory of Coastal Wetland Biogeosciences, China Geologic Survey, Qingdao 266071, Shandong, China

[d] Laboratory for Marine Geology, Qingdao National Laboratory for Marine Science and Technology, Qingdao, 266061, China

[*] Corresponding author at: Key Laboratory of Marine Sedimentology and Environmental Geology, First Institute of Oceanography, SOA, Qingdao 266061, China.
E-mail address: jinxiachen@fio.org.cn (J. Chen); xfshi@fio.org.cn (X. Shi).

ABSTRACT

Coastal vegetation not only mitigates the damage inflicted by marine disasters on coastal area, but also plays an important role in the global carbon cycle (i.e. blue carbon). Nevertheless, detailed records of both long-term changes in coastal vegetation composition and diversity, coupled with climate change and river evolution, remain sparse. To explore vegetation dynamics and their influencing factors on the coastal area of the Bohai Sea (BS) during the Holocene, in this study, we present high-resolution pollen and grain size data obtained from a sediment core of the BS. The results reveal that two rapid and abrupt changes in salt marsh vegetation are linked with the river-system changes. Within each event, a recurring pattern—starting with a decline in Cyperaceae, followed by an increase in *Artemisia* and Chenopodiaceae—suggests a successional process that is determined by the close relationship between Yellow River (YR) channel shifts and the wetland community dynamics. The phreatophyte Cyperaceae at the base of each sequence indicate lower saline conditions. Unchannelized river flow characterized the onset of the YR channel shift, caused a huge river-derived sediment accumulation in the floodplain, and destroyed the sedges in the coastal depression. Along with the formation of a new channel, lateral migration of the lower channel stopped, and a new intertidal mudflat was formed. Pioneer species (Chenopodiaceae, *Artemisia*) were the first to colonize the bare zones of

https://doi.org/10.5194/cp-2020-20
Preprint. Discussion started: 27 February 2020

the lower and middle marsh areas. In addition, the pollen results revealed that the vegetation in the Shandong Peninsula was dominated by broadleaved trees during the early Holocene (8500–6500 a BP) and by conifers and broadleaved forests in the middle Holocene (6500–3500 a BP), which was followed by an expansion of broadleaved trees (3500–1000 a BP). After 1000 a BP, human impacts are recognized as a sudden decrease in *Quercus* and a marked increase in secondary vegetation *Pinus*. The pollen-based temperature index indicated that a warmer early and late Holocene and colder middle Holocene were consistent with previously reported temperature records for North and Northwest China. The main driving factors of temperature variation in this region are insolation, greenhouse gases and the El Niño-Southern Oscillation.

Keywords: Coastal salt marsh; Pollen; Delta superlobe; Temperature; El Niño-Southern Oscillation

1. Introduction

Coastal areas are important habitats for civilizations, and they are playing an increasingly critical role in trade globalization (Hemavathi et al., 2019). Because they are located between marine ecosystems and terrestrial ecosystems, coastal area are prone to many natural hazards such as flooding, storms and tsunamis (Hou and Hou, 2020). Coastal vegetation, which acts as a natural barrier, is widely distributed in coastal areas and could effectively mitigate the damage of marine disasters to the economy and environment of coastal areas (Zhang et al., 2018). Moreover, despite their relatively small global extent (between 0.5 and 1×10^6 km^2), coastal vegetation ecosystems, tidal marshes, mangroves, and seagrasses play an important role in the global carbon cycle (Serrano et al., 2019; Spivak et al., 2019). Their organic carbon sequestration rates exceed those of terrestrial forests, per unit area, by 1–2 orders of magnitude, and contribute ~50% of C sequestered in marine sediments (Serrano et al., 2019). Hence, it is important to understand the long-term spatial–temporal dynamics of coastal vegetation, which are favorable for the global carbon cycle research and coastal restoration.

Climatic fluctuation, post glacial sea-level rise and changes in river discharge provoked dramatic habitat changes along coastal areas during the Late Pleistocene and Holocene (Neumann et al., 2010; Cohen et al., 2012; Pessenda et

https://doi.org/10.5194/cp-2020-20
Preprint. Discussion started: 27 February 2020


Climate of the Past Discussions

al., 2012; Fran ça et al., 2015). Presently, the relationship of sea-level change and coastal vegetation (especially mangrove) evolution has been studied by many researchers (e.g. Engelhart et al., 2007; Gonza ´lez and Dupont, 2009; Fran ça et al., 2012; Woodroffe et al., 2015; Hendy et al., 2016). However, studies on the long-term dynamics of coastal vegetation, coupled with climate change and river evolution, are sparse. The global rivers delivered large amounts of material to the ocean in the Holocene; the total suspended sediment delivered by all rivers to the ocean was approximately 13.5×10^{9} tons annually (Milliman and Meade, 1983). The material transported by the rivers had huge impacts on the coastal ecosystem. Hence, a deeper understanding of correlations between coastal vegetation and river variables is required to better assess coastal vegetation responses to global warming in the future.

In the coastal areas of the BS, vegetation is dominated by warm temperate deciduous broadleaved forests and shrub grasslands (Wang et al., 1993). The YR, as the second largest river in the world in terms of sediment discharge (Milliman and Meade, 1983), transports large amounts of sediment into the BS every year; hence, it has developed a delta complex in the west coastal region of the BS since 7 ka BP (He et al., 2019). Deposition of the Yellow River delta (YRD) complex resulted in the form of a vast area of floodplain and estuarine wetland (Xue et al., 1995; Cui et al., 2009; Liu et al., 2009). Based on the study of coastal vegetation of the BS, it is helpful to understand the spatial and temporal drivers of ecological variability, and thus of the vegetation-climate and river relationship, especially wetland dynamics. However, few related investigations, which can potentially provide a better understanding of the vegetation dynamics and their response to climate and river variables, have been conducted in the Bohai region.

Pollen records have been useful in terms of reconstructing vegetation dynamics and environmental changes associated with climatic changes in the geological record (Bao et al., 2007; Cohen et al., 2008; Giraldo–Giraldo et al., 2018). Therefore, in this study, we carried out a detailed investigation of core sediments from Laizhou Bay, BS. We analyzed pollen and grain size proxies under high resolution and refined the chronology of the core by ^{137}Cs and AMS^{14}C dates. With this in mind, the specific objectives of the current research are formulated as follows: (1) to reconstruct the vegetation evolution history in the Bohai region and (2) to discuss tentatively the effects of climate and environment on coastal vegetation (especially wetlands) during the Holocene.

https://doi.org/10.5194/cp-2020-20
Preprint. Discussion started: 27 February 2020


Climate of the Past Discussions

2. Study area

2.1. Geographical settings

The BS, a shallow inland sea in China, is connected with the Yellow Sea through the narrow Bohai Strait (Figure 1). The main rivers flowing into the BS are the YR, Haihe River, Luanhe River, and Liaohe River. Among these, the YR is the largest and is the main source of sediments in this region. Over the past 2000 years, the YR has annually provided approximately 1.1×10^9 tons of sediment discharged into the BS (Milliman et al., 1987). This immense amount of sediment has resulted in the rapid seaward progradation of YRD, and a rapid change in the location of the main distributaries in the lower delta plain.

The tidal current plays a critical role in the transportation and distribution of sediments in the BS. The tidal currents of the modern BS are dominated by semi-diurnal tides. The velocity of tidal currents varies from 20 to 80 cm/s. Three strong tidal current areas are observed in the northern Bohai Strait, central part of Bohai Bay, and eastern part of Liaodong Bay (Huang et al., 1999). In Laizhou Bay close to the core location, the speed of tidal currents is weak (Gu and Xiu, 1996).

The wind waves off the YRD are dominated by the East Asian monsoon and show significant seasonal variations. The prevailing northerly winds are much stronger in winter than the dominant southerly winds in summer. Strong winter winds induce strong wind waves, and thus cause strong bottom shear stresses which readily erode seabed sediment into water (Yang et al., 2011; Wang et al., 2014; Zhou et al., 2017).

The circulation of the BS is weak and the mean flow velocity is small. In winter, the predominant extension of the Yellow Sea Warm Current (YSWC) intrudes and crosses the Bohai Strait, moving westward along the central part of the BS and splits into two branches. One branch moves toward the northeast to form a clockwise gyre, and the other veers southward and then turns eastward along the southern coast to form a counterclockwise gyre. In summer, the YSWC disappears in the BS. Eddies generated in the BS are stronger than in winter. During this time, the central eddy is missing, the eddy in Laizhou Bay is more pronounced, and the coastal current along the southern and western coastlines of the BS is established (Figure 1b; Liu et al., 2015; Yang et al., 2016).

https://doi.org/10.5194/cp-2020-20
Preprint. Discussion started: 27 February 2020


Climate of the Past Discussions

2.2. Climate and vegetation

The Bohai region lies in a zone of warm temperate monsoonal climate with distinctive seasons. The annual mean air temperature is 7.5–14.0 ℃, and the annual average precipitation is 500–900 mm. As the Liaodong peninsula and Shandong peninsula protrude into the sea, they are clearly influenced by its proximity and experience sufficient rainfall. However, there is less rainfall in the mountain area of the northern part (Wang et al., 1993).

The regional vegetation is dominated by warm temperature deciduous broadleaved forests and shrub grasslands. Currently, natural vegetation only remains in the mountain areas because of widespread anthropogenic activities (e.g. cultivation and farming). The predominant deciduous broadleaved species belong to *Quercus*, such as Q. *liaotungensis*, Q. *dentate*, Q. *acutissima*, and Q. *variabilis*. Co-dominant plants are *Pinus*, including P. *densiflora* that grows in the coastal humid area, and P. *tabulaeformis* that is distributed in the relatively dry North China plain. In the plain area, apart from P. *tabulaeformis*, there are some deciduous broadleaved trees, such as *Ailanthus altissima*, *Koelreuteria paniculata*, and *Morus alba*. Other broadleaved trees, *Betula ermanii*, *Populus tremula*, *Acer* spp., *Tilia amurensis*, and *Carpinus turczaninowii* are distributed in the hills and lowlands (Wang et al., 1993). The coastal wetlands are occupied by herbs and shrubs, such as *Tamarix chinensis*, *Salix matsudana*, *S. integra*, *Phragmites australis*, *Aeluropus Trin*, *Limonium sinense*, *Suaeda glauca*, *Typha orientalis*, and *Acorus calamus* (Li et al., 2007; Xu et al., 2010).

3. Materials and methods

3.1. Core collection, sub–sampling, and chronology

Core CJ06-435 was collected in Laizhou Bay, BS in August 2007 by the R/V *Kan407* of the Shanghai Bureau. The core site is located at 37.50 ℃N, 119.52 ℃E, at a water depth of 14.6 m (Figure 1), with a length of 271 cm. In the laboratory, the core was spilt into two sections, photographed, macroscopically described, and sub-sampled.

Isotopes ^{137}Cs and ^{210}Pb were measured employing EG&G Ortec Gamma Spectrometry at the Nanjing Institute of Limnology and Geography, Chinese Academy of Sciences (NIGLAS). The sediment samples were air-dried and pulverized. ^{137}Cs and ^{210}Pb concentrations were then determined from gamma emissions at 662 and 46.5 keV, respectively. In addition, a total of 10 samples consisting of foraminifera were obtained from the core for radiocarbon

https://doi.org/10.5194/cp-2020-20
Preprint. Discussion started: 27 February 2020


Climate of the Past Discussions

dating. The radiocarbon dating was conducted at the Woods Hole Oceanographic Institution (WHOI) and Beta Analytic Inc., USA. Radiocarbon dates were corrected for the regional marine reservoir effect ($\Delta R = -139 \pm 59$ years, a regional average value determined for the BS) and calibrated using the Calib 7.04 program (Stuiver et al., 2019) with one standard deviation uncertainty ($1.0 \times \sigma$) (Table 1).

3.2. Palynological and grain size sample analysis

A total of 127 samples were selected for pollen analyses. Approximately 3–5 g of bulk sediments were taken from each sample, and a standard tablet of Lycopodium spores was added to each sample to calculate the pollen concentrations. Solutions of 15% HCl and 5% KOH were used to eliminate carbonates and to remove organic matter, respectively. Silicates were removed using 40% HF, and the residue was mounted in glycerin jelly. Fossil pollen was identified and counted with a light microscope at 400× magnification. The percentage of each pollen type was calculated from the total palynomorph sum. The concentration values were calculated using the exotic pollen method, which is the number of pollen grains accumulated in 1.0 g of sediment.

Grain size analysis was performed at 2.0 cm intervals throughout the core using a Malvern Mastersizer 2000 instrument at the laboratory of the First Institute of Oceanography. The chemical procedure of grain size experimental pretreatment was consistent with the procedures described by Chen et al. (2019a). A solution of 30% H_2O_2 and 1.0 mol/l HCl were added to decompose the organic matter and remove carbonates.

4. Results

4.1. Chronological model

Measurements of ^{137}Cs and ^{210}Pb revealed activity at the top of the profile, indicating the recovery of recently deposited sediments. ^{137}Cs is a bomb-derived radionuclide, first appearing in environmental samples at measurable levels around 1954 with the onset of weapon testing (Kirchner and Ehlers, 1998), and was most prevalent in 1963 (the year of maximum fallout from atmospheric weapon testing) (Palinkas and Nittrouer, 2007). Subsurface peaks are not discernible in ^{137}Cs profiles of our study core (Figure 2). However, the deepest onset of ^{137}Cs is an effective marker of

https://doi.org/10.5194/cp-2020-20
Preprint. Discussion started: 27 February 2020


Climate of the Past Discussions

the year 1954 (25 cm).

Often, the combined data of ^{137}Cs and $^{210}Pb_{ex}$ were used to calculate the sedimentation rates (Wu et al., 2015). $^{210}Pb_{ex}$ shows a downward decline owing to the decay of ^{210}Pb when the sediment stably accumulates for an appropriate period, and the $^{210}Pb_{ex}$ activity could be used to calculate the sedimentation rate. However, the $^{210}Pb_{ex}$ profiles of core CJ06-435 did not show a clear downward decline trend (Figure 2), and $^{210}Pb_{ex}$ in the upper parts of the core is not that large when compared with the lower background values. Therefore, the ^{210}Pb data seemed to be unsuitable for estimating the sedimentation rate of core CJ06–435. The ^{137}Cs–derived average sedimentation rate was 0.47 cm/yr in the upper 25 cm of core CJ06–435.

The results of AMS radiocarbon dating are shown in Table 1 and Figure 2. Three samples above the 20 cm depth were not included in the age model because their ^{14}C age was anomalously greater than the ^{137}Cs dating. The calibrated dates of several other samples are plotted against sediment depth and shown in Figure 3.

4.2. Palynology and grain size data

A total of 71 pollen taxa were identified in 127 samples of core CJ06–435. Pollen spectra are dominated by arboreal pollen (AP) in the middle and lower part (271–30 cm) of the core, primarily *Pinus* and *Quercus*. Other common arboreal genera are *Betula*, *Pterocarya*, Ulmaceae, and Moraceae. Nonarboreal pollen (NAP) is dominant in the upper part (30–0 cm) of the core. Among the NAP, Poaceae, Compositae, *Artemisia*, Chenopodiaceae, and Cyperaceae are most common. Fern spores are dominated by *Selaginella sinensis* and Polypodiaceae; however, their content is low throughout the core. CONISS analyses suggest that the pollen diagram can be divided into three zones (Figure 3 and 4).

4.2.1. Palynological zone 1 (271–156 cm)

This zone is characterized by a high content of broad-leaved trees, mostly consisting of *Quercus* (mean 18.7%), *Betula*, *Alnus*, *Pterocarya*, Ulmaceae and Moraceae. The content of conifer pollens is relatively low compared with other zones: *Pinus* ranges from 19.7% to 45.6% (mean 33.6%), and Taxodiaceae is present only occasionally. NAP of

https://doi.org/10.5194/cp-2020-20
Preprint. Discussion started: 27 February 2020


Climate of the Past Discussions

Compositae (mean 1.2%), *Artemisia* (mean 4.2%), and Chenopodiaceae (mean 5.6%) have their lowest percentage in this zone, whereas Cyperaceae (mean 10.3%) and *Typha* (mean 11.2%) show the highest abundance (Figure 3). The palynological concentrations are high, varying between 6050 and 237 grains g^{-1} (Figure 4).

The sediment of this zone is dominated by yellow-brown silt and clay silt with occasional sandy silt layers and shell fragments. The median grain size ranges between 5.3 φ and 7.1 φ, and the average value is approximately 5.9 φ (Figure 2).

4.2.2. Palynological zone 2 (156–30 cm)

This zone can be further divided into four subzones according to the changing components of the pollen types. From 156 to 128 cm (subzone 2a), *Pinus* increases up to the highest abundance (mean 46.6%), whereas the contents of broadleaved trees *Quercus* (16.1–9.5%, mean 14%), *Betula*, *Alnus*, *Pterocarya*, Ulmaceae, and Moraceae declines to different degrees. NAPs of Compositae (mean 2.5%), *Artemisia* (mean 6.6%), and Chenopodiaceae (mean 7.4%) have higher contents, whereas the percentages of Cyperaceae (mean 7.2%) and *Typha* (mean 3.1%) clearly decrease (Figure 3). Total pollen concentration decreases notably in this subzone, especially during the interval of 156–135 cm when the value of total pollen concentrations (62–1306 grains/g, mean 485 grains/g) is the lowest in the entire core (Figure 4).

From 128 to 63 cm (subzone 2b), *Pinus* is present in lower amounts of approximately 49.4–27.3%. The *Betula* content slightly increases; however, the *Quercus* content decreases (18.1–7.9%, mean 13.5%). Small amounts of *Pterocarya*, Ulmaceae, and Moraceae appear occasionally. NAPs of Compositae, *Artemisia*, and Chenopodiaceae continuously increase in this interval to averages of 3.5%, 6.7%, and 12%, respectively. Poaceae, Cyperaceae, and *Typha* were present in largely unchanged proportions compared with subzone 2a (Figure 3). Pollen concentration increases up to a high abundance (mean 1260 grains/g) in this subzone (Figure 4).

From 63 to 41 cm (subzone 2c), the percentage frequency of *Pinus* is reduced upward, whereas that of *Quercus* (17.4–11.8%, mean 14.8%), *Betula*, *Alnus*, *Pterocarya*, and Ulmaceae increases. Similar to subzone 2b, this subzone has relatively high quantities of herb pollen such as Compositae, *Artemisia*, and Chenopodiaceae (Figure 3). Pollen concentrations were found to vary between 456 and 1381 grains/g (Figure 4).

https://doi.org/10.5194/cp-2020-20
Preprint. Discussion started: 27 February 2020


Climate of the Past Discussions

In contrast, pollen subzone 2d (41–30 cm) is marked by a sudden decrease in the broadleaved tree pollen of *Quercus* (9.8%), and a steep increase of the conifer pollen of *Pinus* (41.1%), even though the percentage frequencies of the herbs are the same as those of subzone 2c (Figure 3).

On the basis of the downcore distribution of grain size (Figure 2), zone 2 can be subdivided into three sections. Section 1 (156–135 cm) is characterized by yellow-brown sandy silt mixed with shell fragments. The median grain size ranges between 4.3 φ and 4.8 φ. Section 2 (135–83 cm) is composed mainly of yellow-brown silt with occasional sandy silt layers. Median grain size varies between 5.7 φ and 7.1 φ. Section 3 (83–30 cm) consists of yellow-brown clay silt and sandy silt, with shell fragments at 68–71 cm. The median grain size ranges between 5.3 φ and 6.4 φ.

4.2.3. Palynological zone 3 (30–0 cm)

This zone is characterized by a notable decrease in AP and a rapid increase in NAP. The percentage of *Pinus* and *Quercus* pollens is the lowest in the core, averaging approximately 19.7% and 5.5%, respectively. The content of Poaceae, Compositae, *Artemisia*, and Chenopodiaceae increases in this zone, with average values of *Artemisia* and Chenopodiaceae reaching up to 24.6% and 21.1%, respectively (Figure 3). The total pollen concentration declines to 188 grains/g in the lower part of the zone (30–19 cm) and then increases slightly (to approximately 621 grains/g) at the top (Figure 4).

Based on the change of grain size, zone 3 can be subdivided into two sections. The upper section (30–19 cm) is characterized by soil-yellow sandy silt with many shell fragments occurring at 30–29 cm. The median grain size of the section ranges between 4.3 φ and 5.2 φ. The lower section (19–0 cm, median grain size 5.5 φ–6.8 φ) consists of soil-yellow clay silt with sandy silt layers at some depths (Figure 2).

5. Discussion

5.1. Key terrestrial palynomorphic proxies of environmental and climatic change

In our sediment core CJ06–435, both *Pinus* and *Quercus* pollen are predominant pollen types among the AP. This result is consistent with the pollen records in the surface sediments of Laizhou Bay (Yang et al., 2016). In surface

https://doi.org/10.5194/cp-2020-20
Preprint. Discussion started: 27 February 2020


Climate of the Past Discussions

sediments from Laizhou Bay, higher concentrations of *Pinus* and *Quercus* pollen occur east of Laizhou Bay, and lower concentrations occur in the nearshore area outside the mouth of the YR (Figure 5a and b). This can be explained by the nearshore epicontinental vegetation of Laizhou Bay. In the low mountains and hilly area of Shandong Peninsula, the vegetation is represented chiefly by *Pinus densiflora* and *Quercus* spp. forests (Wang et al., 1993). The surface sediment concentration of *Pinus* and *Quercus* pollen grains is clearly increased near the Shandong Peninsula and is a good indicator of their parental plants on the peninsula. Modern research found that incremental temperature had negative impacts on radial growth of *P. densiflora* and positive impacts on that of *Quercus* spp. (Byun et al., 2013). For example, with the rise of annual mean temperature, *P. densiflora* forests have naturally decreased by approximately 4% in South Korea from 1996 to 2010, while *Quercus* spp. increased by 1.13% (Korea Forest Service, 2011; Kim et al., 2011). Therefore, the variations of *Pinus* and *Quercus* pollen in our sediment core from Laizhou Bay may be related to temperature change.

It is worth noting that *Pinus* pollen is a bisaccate grain. It has relatively high aerodynamic and hydrodynamic characteristics and can be transported efficiently by wind and water (Sander, 2001; Montade et al., 2011). Previous studies revealed that *Pinus* is represented in a small percentage nearshore and in a large percentage in the deep ocean (Zheng et al., 2011; Dai et al., 2014; Dai and Weng, 2015; Luo et al., 2014). Pollen distribution in the surface sediments of Laizhou Bay also shows that *Pinus* pollen decreases seaward along the inflowing rivers; however it increases in a northeasterly direction away from the coast (Yang et al., 2016). Hence, concerning *Pinus* pollen data, caution is required because climate variation alone may not be responsible for the change of *Pinus* pollen in marine sediment. Aerodynamic and hydrodynamic conditions may also influence the value of *Pinus* in sediments.

Herb pollen, especially Chenopodiaceae, also occupies an important position in core CJ06–435 (Figure 3). The spatial distribution of herb pollen suggests that higher concentrations occur in the nearshore area close to the YR estuary and the southwestern part of Laizhou Bay, and low concentrations are found in the east of Laizhou Bay (Figure 5c and d). The YR is the main sediment source of the BS. The annual mean sediment load of the YR was 1.08×10^9 tons before dam construction (Milliman and Meade, 1983), 70–90% of which was deposited and formed a huge delta complex (Zhou et al., 2016). Natural vegetation in the modern YRD includes plenty of wetland herbs Chenopodiaceae

https://doi.org/10.5194/cp-2020-20
Preprint. Discussion started: 27 February 2020


Climate of the Past Discussions

and *Artemisia* (Jiang et al., 2013). Furthermore, under the combined action of the ocean and rivers, alluvial plains and coast plains developed widely along the southern coast of Laizhou Bay. The terrestrial vegetation types in these areas change from a bare intertidal zone to seep weed swamp to reed swamp to cultivated land from the shoreline landward (Xu et al., 2010). Since the transportation distance for herb pollen is normally very short, its pollen concentration in samples close to the mouth of the YR and southwestern part of Laizhou Bay is much higher than in other samples (Figure 5 c and d), indicating that herb pollen of Laizhou Bay is mainly derived from the plant communities of the coastal wetlands. Therefore, we speculated that the herb pollen data in our sediment core might contain some information about the evolution of wetlands.

5.2. Sedimentary records indicative of river channel shifts

The most important geological events in the northern China coast after 7000 a BP were the shift of Yellow River channel and the formation of YRD. The YR has been easily plugged and breached, and therefore its lower reaches migrated because of its huge sediment load. The shifting of the lower reaches of the YR led to the formation of a new delta superlobe (He et al., 2019). Based on a study of cheniers and historical documents, nine YRD superlobes have been proposed by Xue and Cheng (1989) and Xue (1993) on the western shore of the BS. Among these, superlobe 1 (7000–5000 a BP, He et al., 2019), superlobe 7 (11 AD–1048 AD, Xue, 1993), and superlobe 10 (1855 AD–present) are positioned near the core area in this study. The information about these superlobes formation are recorded in our core.

As shown in Figure 3 and 6e, herb percentage abruptly increased at 34 cm and 160 cm. Herb pollen in the sediment of Laizhou Bay is mainly derived from the coastal wetlands of the western BS. In 6000-7000 a BP and 1855 AD, the YR emptied into the BS after a natural course shift, forming two huge delta at the western part of the BS (Saito et al., 2000). Wetland plants are the important vegetation type in the YRD (Jiang et al., 2013). The development of YRD wetland would change the amounts of herb pollen that was transported to the studied site. In addition, the formation of YRD caused the coastline to move closer to the position of the CJ06–435 core. Since most herb plants are small in size, their pollen grains are unable to disperse broadly (Chen et al., 2019b). The migration of the coastline

https://doi.org/10.5194/cp-2020-20
Preprint. Discussion started: 27 February 2020


Climate of the Past Discussions

would change the availability of herb pollen to the studied site, and hence lead to variations of the pollen diagram. Therefore, we concluded that the abrupt change of herb pollen at 160 cm and 34 cm in core CJ06–435 is related to the formation of the YRD superlobe 1 and superlobe 10.

Compared with the pollen percentage, the pollen concentration can be interpreted in different ways. Namely, the percentage of different types of pollen is relative, whereas the pollen concentration is absolute, and it can directly reflect the amounts of pollen that were transported to the study area (Luo et al., 2013). Therefore, it is crucial that a correct interpretation of pollen data is based on a percentage diagram as well as concentration. In core CJ06–435, the concentrations of herbs—especially Chenopodiaceae and *Artemisia* (Figure 6f)—are higher at depths of 160–94 cm (6570–5000 a BP) and 34–0 cm (after 1855 AD), except for the two sections of 160–135 cm and 34–19 cm. A previous study noted that pollen grains would settle out of suspension in the same manner as suspended particles of fine silt and clay (Gail et al., 1999). The grain size data of core CJ06–435 revealed that coarser sediment occurred in the sections of 160–135 cm and 34–19 cm (Figure 6a–d). Therefore, the extremely low pollen concentration in the sections of 160–135 cm and 34–19 cm is closely linked with the coarser sediment. Combined with the results of pollen percentage and grain size, we presumed that the higher herb pollen concentration in the periods of 6570–5000 a BP (160–94 cm) and after 1855 AD (34–0 cm) reflects changes in hydrographic conditions. Pollen data of surface sediments revealed that higher herb pollen concentrations occur in the YR, and the value of these concentrations show a decreasing trend starting from the river mouth towards the ocean. The distribution pattern of surface pollen revealed that the YR is a major carrier for most herbs taxa in the sediment of Laizhou Bay (Yang et al., 2016). At the site of core CJ06–435, which is close to the mouth of the YR in Laizhou Bay, higher herb pollen concentrations in the Holocene samples may indicate increased fluvial discharge.

Sediment grain size provides direct information on changes of the sediment source and the sedimentary environment (Friedman and Sanders, 1978; Wu et al., 2015). The characteristics of grain size can be expressed by the grain size distribution curve, and usually the mean or median diameter is used (Xu, 1999). In this study, the value of mean grain size (Mz) showed that two major grain size boundaries occur at depths of 34 and 19 cm, separating a middle sedimentary unit (34–19 cm) that contains coarser sediment than the lower and upper sedimentary units that

https://doi.org/10.5194/cp-2020-20
Preprint. Discussion started: 27 February 2020


Climate of the Past Discussions

301 contain finer sediment (Figure 6d). At these boundaries, the sand content changes from approximately 15.7% to 39.4%
302 and then to 11.2% (Figure 6a), silt content changes from 59.7–82.1% to 51.5%–58.3% and then to 62.5–75.1% (Figure
303 6b), and clay content changes from 16% to 5.8% and then to 19.8% in an upward direction (Figure 6c). On the basis of
304 ^{137}Cs and ^{210}Pb chronologies (Figure 2), we speculate that these significant changes of grain size parameters at depths
305 of 34 and 17 cm might represent a record of the channel shifts of the YR in 1855 AD and 1976 AD, respectively.
306 The sediment of Laizhou Bay mainly comes from the YR and other small rivers located in the southern part of
307 Laizhou Bay (Zhang et al., 2017; Gao et al., 2018). Prior to 1855 AD, when the YR entered the Yellow Sea, the
308 sediments contribution to the BS of other small rivers was relatively larger. The fine fraction suspension sediment that
309 was derived from other small rivers favors the hypothesis of fine sediment accumulation in core CJ06–435 during this
310 period.
311 When the YR reentered the BS after 1855 AD, the dispersal of YR material contributed substantially to the
312 sedimentation of the BS. It was reported that more than 80% of the YR sediment discharges into the BS during
313 summer (Bi et al., 2011). Owing to the barrier effect of the tidal shear front and the weak river flow, most of the
314 river-delivered sediment is deposited on the offshore delta within 15 km of the river mouth (Wang et al., 2007; Bi et al.,
315 2010). Only a small part of the fine clay fraction is transported by the coastal currents over long distances and
316 deposited across or along the shore in summer time (Wu et al., 2015). During the winter (October to March) season,
317 the much stronger winter monsoon generate large waves, resulting in intensive sediment resuspension in the coastal
318 region owing to the enhanced bottom shear stress (Yang et al., 2011; Bi et al., 2011). The resuspended sediment is
319 transported southeastward along the coast of Laizhou Bay by the monsoon-enhanced coastal currents passing through
320 the location of the sediment core CJ06–435. Therefore, after 1855 AD, the sediment of core CJ06–435 mainly included
321 the fine fraction of the suspended sediment dispersed from the YR mouth, resuspended sediment from the coastal area
322 off the YR delta in the winter, and locally resuspended sediment.
323 The accumulation of YR-suspended sediment during the summer season in Laizhou Bay was closely associated
324 with the sediment dispersion pattern off the active delta lobe (Xing et al., 2016). The estuary of the YR, during most of
325 the period 1855–1976 AD, was north of the modern YRD, and suspended sediment from the YR was transported

https://doi.org/10.5194/cp-2020-20
Preprint. Discussion started: 27 February 2020


Climate of the Past Discussions

northeastward to Bohai Bay and the central Bohai basin. The contribution of YR-suspended sediment to the sedimentation of core CJ06–435 was smaller and the resuspended sediment became a dominant material source. Jiang and Wang (2005) found that the shapes of the sediment grain-size distributions in the YR mouth nearshore area are all characterized by bimodal curves with peaks near 1.2 μm and 30–60 μm. In the offshore area of Laizhou Bay, the sediment grain size is characterized by a mono-modal pattern, and most of the particles are concentrated at peaks near 40–60 μm (Jiang and Wang, 2005). During the winter, the large waves generated by the strong winds may result in intensive resuspension of the seabed sediment and lead to part of the coarse sediment in the YR mouth and Laizhou Bay being transported to the study area, which induces an evident increase in mean grain size and a decrease in the amount of fine grain sized particles. After 1976 AD, the lower channel of the YR shifted to the Qingshuigou course in Laizhou Bay; the suspended sediments derived from the YR estuary were primarily driven southward and southeastward along the coast, leading an increasing transportation of most of the YR-suspended sediment into Laizhou Bay (Qiao et al., 2010). As a result, the dispersal of river-laden sediment contributed substantially to the sedimentation of core CJ06–435, with a fine-grained layer being formed in the upper part of the core.

The results inferred from our grain-size data on the migrations of the YR lower channel since 1855 AD and their effects on the sedimentary environments of the adjacent BS have been proven by some studies from Laizhou Bay (Wu et al., 2015) and central BS (Hu et al., 2011). Based on the records of sediment core collected from Laizhou Bay, Wu et al. (2015) found that when the YR mouth approached the core location, the sediment became finer; otherwise, the active resuspension resulted in the accumulation of coarser sediment owing to strong hydrodynamics. The grain-size results from the central mud areas of the BS also point to the conclusion that the sediment supply from the YR to the central BS was cut off because of the shift of the YR terminal course from the Diaokou source in outer Bohai Bay to the Qingshuigou course in Laizhou Bay in 1976; hence, resuspended sediment became a primary source of sediment dispersal in the central BS. As a result, there was a significant increase in the proportion of sand in surface sediment in the central BS (Hu et al., 2011).

It is worth noting that the variation of grain size characteristics in the period of 6570–5000 a BP is very similar to that after 1855 AD. As shown in Figure 6d, the shift of Mz in the period of 6570–5000 a BP also began with a

https://doi.org/10.5194/cp-2020-20
Preprint. Discussion started: 27 February 2020


Climate of the Past Discussions

significantly increased of Mz at 6570 a BP (160 cm) when the YR flowed into the BS in northern Shangdong province. This similar variation of grain size in the period of 6570-5000 a BP (superlobe 1) and after 1855 AD (superlobe 10) is likely implying a similar YR channel shifting during these two periods. However, more efforts are needed to reveal how the deltaic and neritic sea sedimentary environment was impacted by the river system.

5.3. Coastal salt marsh response to hydrological change

Two high-amplitude salt marsh vegetation shifts are displayed in the herb pollen record during 6570-5000 a BP (superlobe 1) and after 1855 AD (superlobe 10), indicating rapid oscillations of environmental conditions in the coastal area of BS. Within single intervals of the Yellow River superlobe, a recurrent and directional alternation of herb pollen taxa is observed in the following order: the shift of herb pollen data began with an abrupt decrease of Cyperaceae percentages, followed by a steep increase of Chenopodiaceae and *Artemisia* (Figure 7b).

Cyperaceae, Chenopodiaceae, and *Artemisia* are the three plant families/genus that contain the important representatives of coastal salt marsh plants (Lu et al., 2006). In the salt marsh of the modern YRD, species composition of Cyperaceae, Chenopodiaceae, and *Artemisia* varies with salinity and soil moisture. Plant families such as Cyperaceae are mainly composed of hydrophytes and phreatophyte *Heleocharis valleculosa*, *Cyperus rotundus*, *Scirpus planiculmis*, *S. triqueter*, *S. yagara*, *S. juncoides*, and *Juncellus serotinus* (Pan and Xu, 2011). The presence of Cyperaceae necessarily indicates lower saline conditions, since hydrophytes and phreatophyte sedges typically colonize in the middle and upper part of the supralittoral zone, both sides along the riverbank, the coast of the lake, and the interfluvial lowlands of the paleo-river. These areas are far from the coastline, and the main type of soil is salinized soil with lower salinity (Zhang et al., 2009a; Xu, 2011). Chenopodiaceae are mainly composed of halophyte *Suaeda glauca*, *S. salsa*, and *Salicornia europaea*. *Artemisia* mainly consist of halophyte and xerophyte *Artemisia carvifolia*, *A. capillaris*, and *A. annua* (Xing et al., 2003; Zhang et al., 2009b). In the modern YRD, halophyte is distributed in the intertidal zone mudflat and the outside margin part of the supralittoral zone. These areas are near the coastline, characterized by a high incidence of wave brakes and prolonged inundation regimes, and the main type of soil is saline (Zhang et al., 2009b). So, in salt marsh plant communities, the variation of Cyperaceae, Chenopodiaceae, and

https://doi.org/10.5194/cp-2020-20
Preprint. Discussion started: 27 February 2020


Climate of the Past Discussions

Artemisia contents often thought to reflect environmental gradients controlled by the distance from the coast, local topography, terrigenous material and freshwater input (Gonza ́lez and Dupont, 2009; Zhang et al., 2009a). The pollen record from the BS could provide evidence of coastal salt marsh development over decade-to-century of years as a response to environmental alternations during the period of hydrological change.

In the studied sequence, the YR flowed into the BS towards the northern Shandong Province after a course shift. The lower river was initially braided upon relocation, as characterized by unchannelized river flow. At this initial stage, the river-derived sediment was largely accumulated in the floodplain and/or among the antecedent rivers owing to the lack of channelization (Wu et al., 2017), filling the coast of the lake, the interfluvial lowlands of the paleo-river, and the supralittoral zone, etc., causing the destruction of hydrophytes and phreatophyte sedges in these areas. This process is indicated in our records by the significant decrease of Cyperaceae pollen percentages shown for superlobe 1 and superlobe 10 (Figure 7b).

Eventually, natural channel adjustments resulted in the coalescence of multiple channels into a single channel (Wu et al., 2017). A large amount of river-derived sediment was deposited at the mouth of the YR, causing the progradation of the YRD. Upon the original formation of the intertidal zone in the YRD, it was a bare beach wetland, because of strongly influenced by tides. Along with the expansion of new forming beach wetland to migrate seaward, the influence of tides was weakening on the original bare beach wetland and the salinity of original beach wetland was decreasing (Zhang et al., 2007). Pioneer species of salt marshes, e.g., *S. glauca*, *S. salsa* and *Salicornia europaea* (Chenopodiaceae), first colonized this original bare beach wetland (Zhang et al., 2009a). The significant increase of Chenopodiaceae in our pollen record (Figure 7b) is therefore interpreted as the development of the *S. glauca* population.

5.4. Palaeovegetation reconstruction and its climate significance

The palynofloral assemblages (Figure 3) can be used to trace the vegetation successions and climate change around the western BS. As shown in Figure 3 and 4, the vegetation went through six stages of successions.

Vegetation Stage 1 (8500–6500 a BP, 271–156 cm), the palynofloral assemblages are mainly composed of the

https://doi.org/10.5194/cp-2020-20
Preprint. Discussion started: 27 February 2020

pollen of broad-leaved trees, such as *Quercus*, *Betula*, *Alnus*, and Ulmaceae, combined with those of hydrophytes and phreatophyte Cyperaceae and *Typha*, among which, the pollen of *Quercus* and *Typha* are predominant (Figure 3 and 4). In contrast, the pollen of halophytic and xerophytic herbs and conifer trees is scarce. The pollen results suggest that the land area of the western BS was dominated by broadleaved forest and freshwater wetlands, indicating a markedly warmer and wetter climate than the present. The highest values of AP pollen concentration (Figure 4), reflecting a dense vegetation cover, also represent warm conditions during this period. The pollen data are comparable to that found from previous palynological studies carried out in North China (e.g., Yi et al., 2003; Ren, 2007; Chen and Wang, 2012; Sun and Feng, 2015; Hao et al., 2016; Wen et al., 2017) and Northeast China (e.g., Ren and Beug, 2002; Stebich et al., 2015), from which a warm, wet climate corresponding to the Holocene Optimum was inferred. The pollen assemblages encountered herein indicated that the vegetation of the Shandong Peninsula consisted mainly of broadleaved forest, with some conifer trees on the uplands, and freshwater lakes and marshes dominated the coastal area, under the influence of the Holocene climatic optimum.

Vegetation Stage 2a (6500–5900 a BP, 156–128 cm), a climatic cooling period is identified by an increase of conifers, *Pinus*, combined with an abrupt reduction of broadleaved trees. Halophytic and xerophytic herbs taxa such as Compositae, *Artemisia*, and Chenopodiaceae also increase, while Cyperaceae and aquatic herbs *Typha* obviously decrease. The climate shift from warm, wet to cool, and dry may have caused the reduction of broadleaved deciduous forests and the expansion of conifer forests, the freshwater lakes and marshes had spread over the coastal area of BS were gradually disappearing. As introduced in above, a vast imbrication delta complex began to build up at the western part of the BS after 6570 a BP, which resulted in the increase of land area and development of the YR delta wetland. It can be concluded that the expansion of saltbush during this period may be partly related to the formation of the YR delta complex.

Vegetation Stage 2b (5900–3500 a BP, 128–63 cm), the pollen data show that broadleaved trees such as *Quercus*, *Pterocarya*, Ulmaceae and Moraceae were fewer during this period, whereas halophytic and xerophytic herbs (*Artemisia* and Chenopodiaceae) increased (Figure 3 and 4) compared with the previous period. These associations may indicate cooler and drier climatic conditions.

https://doi.org/10.5194/cp-2020-20
Preprint. Discussion started: 27 February 2020


Climate of the Past Discussions

Vegetation Stage 2c (3500–1000 a BP, 63–41 cm), a warm climatic phase occurred, as suggested by the increase in representatives of broadleaved trees (*Quercus*, *Betula*, *Alnus*, *Pterocarya*, and Ulmaceae), with low frequencies of conifer pollen (*Pinus*) throughout the interval. Moreover, halophytic and xerophytic herb pollen, including Compositae, *Artemisia*, and Chenopodiaceae, still occurred with high frequency (Figure 3 and 4). Accordingly, the assemblages reveal that a warm, dry climate probably developed during the late Holocene. Based on 73 selected globally distributed Holocene temperature records, Marcott et al. (2013) found a global mean temperature pattern with a warmer early and middle Holocene (ca. 10000-5000 a BP) followed by a long-term cooling trend towards the late Holocene. However, many Holocene temperature records from central Asia (Aizen et al., 2016; Huang et al., 2015; Rao et al., 2019), the Tibetan Plateau (Thompson et al., 1997; Zhao et al., 2013), and North China (Jiang et al., 2006) revealed an irreconcilable conflict with the synthesized record of Marcott et al. (2013). These records indicated a warm early Holocene from ca. 10000 to 7000–6000 a BP, a cold mid-Holocene from ca. 7000–6000 to 4000–3000 a BP, and then a warming late Holocene from ca. 3000–4000 a BP to the present, consistent with the basic change pattern of our temperature record.

Vegetation Stage 2d (1000 a BP–after 1855 AD, 41–30 cm), there is a dramatic decrease in the occurrence of *Quercus*, quickly followed by a sudden increase in *Pinus* (Figure 3 and 4). These pollen data suggest that the previous warm temperature deciduous broadleaved forests dominated by *Quercus* were replaced by secondary vegetation *Pinus* under anthropogenic influence. This assumption is supported by previous palynological studies. Yi et al. (2003) found a sudden reduction of *Quercus*, followed by a marked increase of *Pinus* after 1300 a BP at the YRD. Their research considered that this typical lag between the two taxa may indicate that, after the clearance of the local broadleaved deciduous forests, the vegetation was replaced by a secondary pine forest. Park and Kim (2015) also interpreted the decrease in the percentage of *Quercus* and increase of *Pinus* in the late Holocene as marking the development of secondary vegetation under anthropogenic influence.

Vegetation Stage 3 (after 1855 AD, 30–0 cm), a significant decline in broadleaved trees (*Quercus*) and conifers (*Pinus*) pollen, as well as an increase in the frequency of herbs (Poaceae, Compositae, *Artemisia*, and Chenopodiaceae) pollen may reflect the further strengthening of human disturbance on the vegetation and the expansion of intensive

https://doi.org/10.5194/cp-2020-20
Preprint. Discussion started: 27 February 2020


Climate of the Past Discussions

agricultural cultivation into forests of the BS coastal area. Moreover, after 1855 AD, the present YR began returning to the BS, and forming a vast area of floodplain and estuarine wetland on the southwest coast of the BS (Saito et al., 2000; Jiang et al., 2013). The variation of herb pollen may be partly related to the development of the modern YRD wetland.

5.5. Holocene temperature variations in North China and possible driving mechanisms

As shown in Figure 8b, the *Quercus* pollen percentage of core CJ06-435, as a temperature index, exhibits a warm early Holocene from 8500 to 6500 a BP, a cool mid-Holocene from 6500 to 3500 a BP, and then a relatively warm late Holocene from 3500 to 1000 a BP. After 1000 a BP, the strengthening of human activity destroyed the natural vegetation of the study area, and the temperature could not be reconstructed by our pollen results. This temperature record is reasonably corroborated by four recently-published and relatively well-dated sequences from North China, Northwest China, and the Tibetan Plateau (see Figure 1a for site locations), including the sedimentary pollen-based temperature record from the Narenxia Peat within the Kanas Lake, Northwest China (Figure 8c; Feng et al., 2017); the Guliya ice core $\delta^{18}O$ record from the western Kunlun Shan, southwestern Tibetan Plateau (Figure 8d; Thompson et al., 1997); alpine peat α-cellulose $\delta^{13}C$ record from the Altai Mountains in Northwest China (Figure 8e; Rao et al., 2019); and lacustrine sedimentary pollen-based quantitative temperature record (the mean annual temperature) from Lake Bayanchagan in Inner Mongolia in North China (Figure 8f; Jiang et al., 2006). All four records indicate that the temperature was high between 8500 and 6000 a BP, low between 6000 and 3000–4000 a BP, and averagely high during the past 3000–4000 a BP (Figure 8c–f), consistent with the basic change pattern of our pollen-based temperature index (Figure 8b). The comparison of the five records demonstrates that the CJ06-435 core *Quercus* pollen percentage record is, at a minimum, of regional significance.

Insolation has been widely accepted as an important factor in Holocene climate variation. The covariation of Northern Hemisphere extratropics (30 °to 90 °N) temperature and local summer insolation on an orbital scale, and the long-term decrease of summer insolation make the especially pronounced cooling of the Northern Hemisphere extratropics during the Holocene (Marcott et al., 2013) appear reasonable. However, the general pattern of temperature variation revealed by our study is not entirely consistent with local mean annual insolation forcing (Figure 8a). Our

https://doi.org/10.5194/cp-2020-20
Preprint. Discussion started: 27 February 2020


Climate of the Past Discussions

476 results indicated a cold mid-Holocene from 6500 to 3500 a BP and a relatively warm late Holocene. This temperature
477 characterization of a cool mid-Holocene and a relatively warm late-Holocene is also seen in many proxy records in the
478 North and Northwest China (Thompson et al., 1997; Jiang et al., 2006; Aizen et al., 2016; Hou et al., 2016; Feng et al.,
479 2017; Rao et al., 2019). Furthermore, $\delta^{18}O$ data of permafrost ice wedges from the Lena River Delta in the Siberian
480 Arctic reflect warming winter season temperature over the past 7000 years (Meyer et al., 2015). Therefore, forcings
481 other than Northern Hemisphere insolation are required to explain the cooler mid-Holocene seen in the mid-high
482 latitudes of continental Eurasia. Two such possible forcings are the changes in greenhouse gases (GHG) concentrations
483 and variations of El Niño-Southern Oscillation (ENSO) activities.

484 Radiative forcing by GHG rose 0.5 W/m^2 during the mid-late Holocene (Marcott et al., 2013), which would be
485 expected to yield 1° C warming at Kinderlinskaya Cave in the southern Ural Mountains from 7 ka to the pre-industrial
486 (Baker et al., 2017). Recently, both winter insolation and GHG forcing have been proposed as the major driving factors
487 for winter warming during the past 7 ka in the Siberian Arctic (Meyer et al., 2015) and the southern Ural Mountains
488 (Baker et al., 2017). Similarly, summer warming in central Asia during the mid-late Holocene, recorded by the alpine
489 peat α-cellulose $\delta^{13}C$ record from the Altai mountains (Rao et al., 2019), has been proposed to be mainly driven by the
490 enhanced GHG forcing and strengthened human activities. Hence, it appears that GHG forcing is an important driver
491 for mid-late Holocene temperature variations.

492 We compared our pollen-based temperature index (Figure 8b) with the frequency of El Niño events reconstructed
493 from the Botryococcene concentration in the El Junco Lake sediment (Figure 8g; Zhang et al., 2014) and the ENSO
494 variability reconstructed from $\delta^{18}O$ values of individual planktonic foraminifera retrieved from deep-sea sediments
495 (Figure 8h; Koutavas and Joanides, 2012). As shown in Figure 8, lower temperature periods in mid-Holocene tend to
496 occur during a period of low El Niño activity, which indicates that some link may exist between the temperature of
497 Shandong Peninsula and the ENSO system. Modern research suggested that ENSO can influence the evolution of
498 temperature behavior (Triacca et al., 2014). In East Asia, the strength of winter monsoon and East Asia troughs
499 weakens in an El Niño year, and the weakening could cause the observed winter half-year warming (Xu et al., 2005).
500 At a millennial time scale, using pollen data from Lake Moon in the central part of the Great Khingan Mountain Range,

https://doi.org/10.5194/cp-2020-20
Preprint. Discussion started: 27 February 2020

Wu et al. (2019) have recently connected increased El Niño frequency with the shrinkage of winter monsoon activity in the East Asia, and the warming of winter temperature in the Great Khingan Mountain Range since the mid-Holocene. Likewise, the results of this study, indicating more or less synchronicity of the climate change at Shandong Peninsula and ENSO activity, provide a possible linkage between North China climate and oceanic forcing during mid-late Holocene.

In summary, the temperature characterizations of a cool mid-Holocene and a relatively warm late-Holocene revealed by the mid-high latitudes of continental Eurasia records can be explained by the change of insolation, GHG forcing and ENSO activity. The cooler mid-Holocene may be related to a combination of the decreasing summer insolation, relatively lower GHG radiative forcing, and weak El Niño activity during this interval. Along with enhanced GHG forcing and strengthened ENSO activity in the late Holocene, there was increased temperature.

6. Conclusions

Through the palynological and grain size reconstruction of coastal area vegetation and environment in core CJ06–435, we were able to identify specific responses of plant communities to climatic (temperature, precipitation), hydrological (YR), and anthropogenic impacts. Our data elucidate the pattern and mechanisms driving coastal salt marsh succession at decade-to-century timescales. Two intervals of expanded salt marsh vegetation correspond to the formation of YR delta superlobes, indicating that soil development and salinity gradients are the main factors determining the vegetation dynamics of coastal wetland. Our pollen-based temperature index revealed a warm early Holocene (8500–6500 a BP), a subsequent cool stage between 6500 and 3500 a BP, and a warm episode from 3500 to 1000 a BP. The reliability of the record, especially the cooler mid-Holocene, is further supported by the other several temperature records from North China, Northwest China, and the Tibetan Plateau. We suggest that changes in insolation, GHG forcing, and ENSO activity could have played an important role in the temperature evolution at the mid-high latitudes of continental Eurasia.

https://doi.org/10.5194/cp-2020-20
Preprint. Discussion started: 27 February 2020


Climate of the Past Discussions

Code/Data availability

The co-authors declare that all data included in this study are available upon request by contact with the corresponding author (Email: *jinxiachen@fio.org.cn*).

Author contribution

Jinxia Chen wrote the manuscript; Xuefa Shi and Yanguang Liu revised the manuscript many times; Shuqing Qiao provided many constructive suggestions for the manuscript, Shixiong Yang, Shijuan Yan, Huahua Lv, Xiaoyan Li and Chaoxin Li provided financial support for the collection of samples and obtained samples.

Competing interests

The authors declare that they have no conflict of interest.

Acknowledgements

We thank the shipboard teams of the R/V *Kan407* for sampling. We also thank Dr. Nan Qingyun for improving this paper. This work was supported by the National Natural Science Foundation of China (Grant Nos. 41420104005 and 41576054).

References

Aizen, E.M., Aizen, V.B., Takeuchi, N., Mayewski, P.A., Grigholm, B., Joswiak, D.R., Nikitin, S.A., Fujita, K., Nakawo, M., Zapf, A., Schwikowshi, M.: Abrupt and moderate climate changes in the mid-latitudes of Asia during the Holocene, J.

https://doi.org/10.5194/cp-2020-20
Preprint. Discussion started: 27 February 2020

Glaciol., 62, 411–439, 2016.

Bao, R., Alonso, A., Delgado, C., Pagés, J.L.: Identification of the main driving mechanisms in the evolution of a small coastal wetland (Traba, Galicia, NW Spain) since its origin 5700 cal yr BP, Palaeogeogr. Palaeoclimatol. Palaeoecol., 247, 296–312, 2007.

Baker, J.L., Lachniet, M.S., Chervyatsova, O., Asmerom, Y. & Polyak, V.: Holocene warming in western continental Eurasia driven by glacial retreat and greenhouse forcing, Nat. Geosci., https://doi.org/10.1038/NGEO2953, 2017.

Bi, N.S., Yang, Z.S., Wang, H.J., Hu, B.Q., Ji, Y.J.: Sediment dispersion pattern off the present Huanghe (Yellow River) subdelta and its dynamic mechanism during normal river discharge period, Estuar. Coast. Shelf. S., 86, 352–362, 2010.

Bi, N.S., Yang, Z.S., Wang, H.J., Fan, D.J., Sun, X.X., Lei, K.: Seasonal variation of suspended-sediment transport through the southern Bohai Strait, Estuar. Coast. Shelf. S., 93, 239–247, 2011.

Byun, J.G., Lee, W.K., Kim, M., Kwak, D.A., Kwak, H., Park, T., Byun, W.H., Son, Y., Choi, J.K., Lee, Y.J., Saborowski, J., Chung, D.J., Jung, J.H.: Radial growth response of Pinus densiflora and Quercus spp. To topographic and climatic factors in South Korea, J. Plant. Ecol., 6, 380–392, 2013.

Chen, J.X., Nan, Q.Y., Li, T.G., Sun, R.T., Sun, H.J., Lu, J.: Variations in the East Asian winter monsoon from 3500 to 1300 cal. yr BP in northern China and their possible societal impacts, J. Asian Earth Sci, https://doi.org/10.1016/j.jseaes.2019.103912, 2019a.

Chen, J.X., Li, T.G., Nan, Q.Y., Shi, X.F., Liu, Y.G., Jiang, B., Zou, J.J., Selvaraj, K., Li, D.L., Li, C.S.: Mid-late Holocene rainfall variation in Taiwan: A high-resolution multiproxy record unravels the dual influence of the Asian monsoon and ENSO, Palaeogeogr. Palaeoclimatol. Palaeoecol., 516, 139–151, 2019b.

Chen, W., Wang, W.M.: Middle-Late Holocene vegetation history and environment changes revealed by pollen analysis of a core at Qingdao of Shandong Province, East China, Quat. Int., 254, 68–72, 2012.

Cohen, M.C.L., Lara, R.J., Smith, C.B., Angélica, R.S., Dias, B.S., Pequeno, T.: Wetland dynamics of Marajó Island, northern Brazil, during the last 1000 years, Catena, 76(1), 70–77, 2008.

Cohen, M.C.L., Pessenda, L.C.R., Behling, H., Rossetti, D.d.F., França, M.C., Guimarães, J.T.F., Friaes, Y., Smith, C.B.: Holocene palaeoenvironmental history of the Amazonian mangrove belt, Quat. Sci. Rev., 55, 50–58, 2012.

Cui, B.S., Yang, Q.C., Yang, Z.F., Zhang, K.J.: Evaluating the ecological performance of wetland restoration in the Yellow River Delta, China, Ecol. Eng. 35, 1090–1103. 2009.

Dai, L., Weng, C.Y., Lu, J., Mao, L.M.: Pollen quantitative distribution in marine and fluvial surface sediments from the northern South China Sea: new insights into pollen transportation and deposition mechanisms, Quat. Int., 325, 136–149, 2014.

Dai, L., Weng, C.Y.: Marine palynological record for tropical climate variations since the late last glacial maximum in the northern South China Sea, Deep-sea. Res. Pt. II., 122, 153-162, 2015.

Engelhart, S.E., Horton, B.P., Roberts, D.H., Bryant, C.L., Corbett, D.R.: Mangrove pollen of Indonesia and its suitability as a sea-level indicator, Mar. Geol., 242, 65–81, 2007.

Feng, Z.D., Sun, A.Z., Abdusalih, N., Ran, M., Kurban, A., Lan, B., Zhang, D.L., Yang, Y.P.: Vegetation changes and associated climatic changes in the southern Altai Mountains within China during the Holocene, Holocene, 27(5), 683–693, 2017.

https://doi.org/10.5194/cp-2020-20
Preprint. Discussion started: 27 February 2020

França, M.C., Francisquini, M.I., Cohen, M.C.L., Pessenda, L.C.R., Rossetti, D.F., Guimarães, J.T.F., Smith, C.B.: The last mangroves of Marajó Island–Eastern Amazon: Impact of climate and/or relative sea-level changes, Rev. Palaeobot. Palyno., 187, 50–65, 2012.

França, M.C., Alves, I.C.C., Castro, D.F., Cohen, M.C.L., Rossetti, D.F., Pessenda, L.C.R., Lorente, F.L., Fontes, N.A., Junior, A.Á.B., Giannini, P.C.F., Francisquini, M.I.: A multi-proxy evidence for the transition from estuarine mangroves to deltaic freshwater marshes, Southeastern Brazil, due to climatic and sea-level changes during the late Holocene, Catena, 128, 155–166, 2015.

Friedman, G.M., Sanders, J.E.: Principles of sedimentology, John Wiley and Sons, Inc, 1–792, 1978.

Gail, L.C., Alexei, S., Ian, D.C.: Pollen transport through distributaries and depositional patterns in coastal waters, Palaeogeogr. Palaeoclimatol. Palaeoecol, 149, 257–270, 1999.

Gao, M.S., Guo, F., Hou, G.H., Qiu, J.D., Kong, X.H., Liu, S., Huang, X.Y., Zhuang, H.H.: The evolution of sedimentary environment since late Pleistocene in Laizhou Bay, Bohai Sea, Geol. Chin., 45(1), 59–68, 2018. (in Chinese with English abstract)

Giraldo-Giraldo, M.J., Velásquez-Ruiz, C.A., Pardo-Trujillo, A.: Late-Holocene pollen-based paleoenvironmental reconstruction of the El Triunfo wetland, Los Nevados National Park (Central Cordillera of Colombia), Holocene, 28(2), 183–194, 2018.

Gonzalez, C., Dupont, L.M.: Tropical salt marsh succession as sea-level indicator during Heinrich events, Quat. Sci. Rev., 28, 939–946, 2009.

Gu, Y.H., Xiu, R.C.: On the current and storm flow in the Bohai Sea and their role in transporting deposited silt of the Yellow River, J. Oceanogr. Huanghai & Bohai Seas., 14(1), 1–6, 1996.

Hao, Q., Liu, H.Y., Liu, X.: Pollen-detected altitudinal migration of forests during the Holocene in the mountainous forest–steppe ecotone in northern China, Palaeogeogr. Palaeoclimatol. Palaeoecol., 446, 70–77, 2016.

He, L., Xue, C.T., Ye, S.Y., Amorosi, A., Yuan, H.M., Yang, S.X., Laws, E.A.: New evidence on the spatial-temporal distribution of superlobes in the Yellow River Delta Complex, Quat. Sci. Rev., 214, 117–138, 2019.

Hemavathi, S., Manjula, R., Ponmani, N.: Numerical Modelling and Experimental Investigation on the Effect of Wave Attenuation Due to Coastal Vegetation, Proceedings of the Fourth International Conference in Ocean Engineering (ICOE2018), 23, 99–110, 2019.

Hendy, I.L., Minckley, T.A., Whitlock, C.: Eastern tropical Pacific vegetation response to rapid climate change and sea level rise: A new pollen record from the Gulf of Tehuantepec, southern Mexico, Quat. Sci. Rev., 145, 152–160, 2016.

Hou, J.Z., Huang, Y.S., Zhao, J.T., Liu, Z.H., Colman, S., An, Z.S.: Large Holocene summer temperature oscillations and impact on the peopling of the northeastern Tibetan Plateau, Geophys. Res. Lett., 43, 1323–1330, 2016.

Hou, W., Hou, X.Y.: Spatial–temporal changes in vegetation coverage in the global coastal zone based on GIMMS NDVI3g data, Int. J. Remote. Sens., 41(3), 1118–1138, 2020.

Hu, L.M., Guo, Z.G., Shi, X.F., Qin, Y.W., Lei, K., Zhang, G.: Temporal trends of aliphatic and polyaromatic hydrocarbons in the Bohai Sea, China: Evidence from the sedimentary record, Org. Geochem., 42, 1181–1193, 2011.

Huang, D.J., Su, J.L., Backhaus, J.O.: Modelling the seasonal thermal stratification and baroclinic circulation in the Bohai Sea, Cont. Shelf. Res., 19, 1485–1505, 1999.

https://doi.org/10.5194/cp-2020-20
Preprint. Discussion started: 27 February 2020

Huang, X.Z., Chen, C.Z., Jia, W.N., An, C.B., Zhou, A.F., Zhang, J.W., Jin, M., Xia, D.S., Chen, F.H., Grimm, E.C.: Vegetation and climate history reconstructed from an alpine lake in central Tienshan Mountains since 8.5 ka BP, Palaeogeogr. Palaeoclimatol. Palaeoecol., 432, 36–48, 2015.

Jiang, W.S., Wang, H.J.: Distribution of suspended matter and its relationship with sediment particle size in Laizhou Bay, Oceanol. Limnol. Sin., 36(2), 97–103, 2005.

Jiang, W.Y., Guo, Z.T., Sun, X.J., Wu, H.B., Chu, G.Q., Yuan, B.Y., Hatte, C., Guiot, J.: Reconstruction of climate and vegetation changes of Lake Bayanchagan (Inner Mongolia): Holocene variability of the east Asian monsoon, Quat. Res., 65, 411–420, 2006.

Jiang, D.J., Fu, X.F., Wang, K.: Vegetation dynamics and their response to freshwater inflow and climate variables in the Yellow River Delta, China, Quat. Int., 304, 75–84, 2013.

Kim, C., Park, J.H., Jang, D.H.: Changes of the forest types by climate changes using satellite imagery and forest statistical data: a case in the Chungnam Coastal Ares, Korea, J. Environ. Impact. Asses., 20, 523–538, 2011.

Kirchner, G., Ehlers, H.: Sediment Geochronology in Changing Coastal Environments: Potentials and Limitations of the ^{137}Cs and ^{210}Pb Methods, J. Coast. Res., 14, 483–492, 1998.

Korea Forest Service: Statistical Yearbook of Forestry. Daejeon, Korea: KFS, 2011.

Koutavas, A., Joanides, S.: El Niño-Southern Oscillation extrema in the Holocene and Last Glacial Maximum, Paleoceanography, https://doi.org/10.1029/2012PA002378, 2012.

Li, C.Y., Yan, L.Q., Han, T.X.: Research on composition of wetland vegetation in Shandong, Shandong Forest Sci. Tech., 4, 27–29, 2007. (in Chinese with English abstract)

Liu, W.Z., Zhang Q.F., Liu, G.H.: Seed banks of a river–reservoir wetland system and their implications for vegetation development, Aquat. Bot., 90, 7–12, 2009.

Liu, D.Y., Li, X., Emeis, K.C., Wang, Y,J., Richard, P.: Distribution and sources of organic matter in surface sediments of Bohai Sea near the Yellow River Estuary, China, Estuar. Coast. Shelf. S., 165, 128–136, 2015.

Lu, J.J., He, W.S., Tong, C.F., Wang, W.: Wetland Ecology. Higher Education Press, Beijing, 2006.

Luo, C.X., Chen, M.H., Xiang, R., Liu, J.G., Zhang, L.L., Lu, J., Yang, M.X.: Characteristics of modern pollen distribution in surface sediment samples for the northern South China Sea from three transects, Quat. Int., 286, 148–158, 2013.

Luo, C.X., Chen, M.H., Xiang, R., Liu, J.G., Zhang, L.L., Lu, J., Yang, M.X.: Modern pollen distribution in marine sediments from the northern part of the South China Sea, Mar. Micropaleontol., 108, 41–56, 2014.

Marcott, S.A., Shakun, J.D., Clark, P.U., Mix, A.C.: A reconstruction of regional and global temperature for the past 11,300 years, Science, 339, 1198–1201, 2013.

Meyer, H., Opel, T., Laepple, T., Dereviagin, A.Y., Hoffmann, K., Werner, M.: Long-term winter warming trend in the Siberian Arctic during the mid- to late Holocene, Nat. Geosci., https://doi.org/ 10.1038/NGEO2349, 2015.

Milliman, J.D., Meade, R.H.: World-wide delivery of river sediment to oceans, J. Geol., 91, 1–21, 1983.

Milliman, J.D., Qin, Y.S., Ren, M.E., Saito, Y.: Man's influence on the erosion and transport of sediment by Asian rivers: the Yellow River (Huanghe) example, J. Geol., 95, 751–762, 1987.

Montade, V., Nebout, N.C., Kissel, C., Mulsow, S.: Pollen distribution in marine surface sediments from Chilean Patagonia, Mar. Geol., 282, 161–168, 2011.

https://doi.org/10.5194/cp-2020-20
Preprint. Discussion started: 27 February 2020


Climate of the Past Discussions

662 Neumann, F.H., Scott, L., Bousman, C.B., As, L.V.: A Holocene sequence of vegetation change at Lake Eteza, coastal
663 KwaZulu-Natal, South Africa, Rev. Palaeobot. Palyno., 162, 39–53, 2010.
664 Pan, Y., Xu, J.W.: Studies on Resource and Flora of Aquatic Vascular Plants in Wetland of Yellow River Delta, J. Anhui Agr.
665 Sci., 39(3), 1642–1644, 2011. (in Chinese with English abstract)
666 Palinkas, C.M., Nittrouer, C.A.: Modern sediment accumulation on the Po shelf, Adriatic Sea, Cont. Shelf Res., 27, 489–505,
667 2007.
668 Park, J., Kim, M.: Pollen-inferred late Holocene agricultural developments in the vicinity of Woljeong-ri, southwestern
669 Korea, Quat. Int., 384, 13–21, 2015.
670 Pessenda, L.C.R., Vidotto, E., Oliveira, P.E.D., Jr, A.A.B., Cohen, M.C.L., Rossetti, D.d.F., Ricardi-Branco, F., Bendassolli,
671 J.A.: Late Quaternary vegetation and coastal environmental changes at Ilha do Cardoso mangrove, southeastern Brazil.
672 Palaeogeogr, Palaeoclimatol. Palaeoecol., 363–364, 57–68, 2012.
673 Qiao, S.Q., Shi, X.F., Zhu, A.M., Liu, Y.G., Bi N.S., Fang, X.S., Yang, G.: Distribution and transport of suspended sediments
674 off the Yellow River (Huanghe) mouth and the nearby Bohai Sea, Estuar. Coast. Shelf. S., 86, 337–344, 2010.
675 Rao, Z.G., Huang, C., Xie, L.H., Shi, F.X., Zhao, Y., Cao, J.T., Gou, X.H., Chen, J.H., Chen, F.H.: Long-term summer
676 warming trend during the Holocene in central Asia indicated by alpine peat a-cellulose $\delta^{13}C$ record, Quat. Sci. Rev., 203,
677 56–67, 2019.
678 Ren, G.Y., Beug, H.J.: Mapping Holocene pollen data and vegetation of China, Quat. Sci. Rev., 21, 1395–1422, 2002.
679 Ren, G.Y.: Changes in forest cover in China during the Holocene, Veget. Hist. Archaeobot., 16, 119–126, 2007.
680 Saito, Y., Wei, H.L., Zhou, Y.Q., Nishimura, A., Sato, Y., Yokota, S.: Delta progradation and chenier formation in the
681 Huanghe (Yellow River) delta, China, J. Asian Earth Sci., 18, 489–497, 2000.
682 Sander, V.D.K.: Pollen distribution in marine sediments from the south-eastern Indonesian waters, Palaeogeogr.
683 Palaeoclimatol. Palaeoecol., 171, 341–361, 2001.
684 Serrano, O., Lovelock, C.E., Atwood, T.B., Macreadie, P.I., Canto, R., Phinn, S., Arias-Ortiz, A., Bai, L., Baldock, J., Bedulli,
685 C., et al.: Australian vegetated coastal ecosystems as global hotspots for climate change mitigation, Nat. Commun.,
686 https://doi.org/10.1038/s41467–019–12176–8, 2019.
687 Spivak, A.C., Sanderman, J., Bowen, J.L., Canuel, E.A., Hopkinson, C.S.: Global-change controls on soil-carbon
688 accumulation and loss in coastal vegetated ecosystems, Nat. Geosci., 12, 685–692, 2019.
689 Sun, A.Z., Feng, Z.D.: Climatic changes in the western part of the Chinese Loess Plateau during the Last Deglacial and the
690 Holocene: A synthesis of pollen records, Quat. Int., 372, 130–141, 2015.
691 Stebich, M., Rehfeld, K., Schlütz, F., Tarasov, P.E., Liu, J.Q., Mingram, J.: Holocene vegetation and climate dynamics of NE
692 China based on the pollen record from Sihailongwan Maar Lake, Quat. Sci. Rev., 124, 275–289, 2015.
693 Stuiver, M., Reimer, P.J., Reimer, R.W.: CALIB 7.1 [WWW program, http://calib.org], 2019.
694 Thompson, L.G., Yao, T.D., Davis, M.E., Henderson, K.A., Mosley-Thompson, E., Lin, P.N., Beer, J., Synal, H.-A.,
695 Cole-Dai, J., Bolzan, J.F.: Tropical climate instability: the last glacial cycle from a Qinghai-Tibetan ice core, Science,
696 276, 1821–1825, 1997.
697 Triacca, U., Pasini, A., Attanasio, A., Giovannelli, A., Lippi, M.: Clarifying the Roles of Greenhouse Gases and ENSO in
698 Recent Global Warming through Their Prediction Performance, J. Clim., 27, 7903–7910, 2014.

https://doi.org/10.5194/cp-2020-20
Preprint. Discussion started: 27 February 2020


Climate of the Past Discussions

699 Wang, K.F. and others: Spore-pollen and algal assemblages in the sediments of the Bohai Sea and palaeoenvironments.
700 Geological Publishing House, Beijing, 1993.
701 Wang, H., Yang, Z., Li, Y., Guo, Z., Sun, X., Wang, Y.: Dispersal pattern of suspended sediment in the shear frontal zone off
702 the Huanghe (Yellow River) mouth, Cont. Shelf Res., 27, 854–871, 2007.
703 Wang, H.J., Wang, A.M., Bi, N.S., Zeng, X.M., Xiao, H.H.: Seasonal distribution of suspended sediment in the Bohai Sea,
704 China, Cont. Shelf Res., 90, 17–32, 2014.
705 Wen, R.L., Xiao, J.L., Fan, J.W., Zhang, S.R., Yamagata, H.: Pollen evidence for a mid-Holocene East Asian summer
706 monsoon maximum in northern China, Quat. Sci. Rev., 176, 29–35, 2017.
707 Woodroffe, S.A., Long, A.J., Milne, G.A., Bryant, C.L., Thomas, A.L.: New constraints on late Holocene eustatic sea-level
708 changes from Mahe, Seychelles, Quat. Sci. Rev., 115, 1–16, 2015.
709 Wu, X., Bi, N.S., Kanai, Y., Saito, Y., Zhang, Y., Yang, Z.S., Fan, D.J., Wang, H.J.: Sedimentary records off the modern
710 Huanghe (Yellow River) delta and their response to deltaic river channel shifts over the last 200 years, J. Asian Earth
711 Sci., 108, 68–80, 2015.
712 Wu, X., Bi, N.S., Xu, J.P., Nittrouer, J.A., Yang, Z.S., Saito, Y., Wang, H.J.: Stepwise morphological evolution of the active
713 Yellow River (Huanghe) delta lobe (1976–2013): Dominant roles of riverine discharge and sediment grain size,
714 Geomorphology, https://doi.org/10.1016/ j.geomorph.2017.04.042, 2017.
715 Wu, J., Liu, Q., Cui, Q. Y., Xu, D. K., Wang, L., Shen, C. M., Chu, G.Q., Liu, J.Q.: Shrinkage of East Asia winter monsoon
716 associated with increased ENSO events since the mid-Holocene, J. Geophys. Res., 124, 3839–3848, 2019.
717 Xing, S.Y., Xi, J.B., Zhang, J.F., Song, Y.M., Ma, B.Y.: The basic characteristics and the main types of vegetation in the
718 Yellow River delta region, J. Northeast Forest. Univ., 31(6), 85–86, 2003. (in Chinese)
719 Xing, G.P., Wang, H.J., Yang, Z.S., Bi, N.S.: Spatial and temporal variation in erosion and accumulation of the subaqueous
720 Yellow River delta (1976-2004), J. Coast. Res., 74, 32–47, 2016.
721 Xu, J.X.: Grain-size characteristics of suspended sediment in the Yellow River, China, Catena, 38, 243–263, 1999.
722 Xu, W.C., Ma, J.s., Wang, W.: A review of studys on the influence of ENSO events on the climate in China, Sci. Meteorol.
723 Sin., 25(2), 212–220, 2005.
724 Xu, Z.J., Zhang, X.L., Zhang, Z.H., Zhang, W.: Analysis of the biodiversity characters of coastal wetlands in southern
725 Laizhou Bay, Ecol. Env. Sci., 19(2), 367–372, 2010. (in Chinese with English abstract)
726 Xu, J.W.: Research on Diversity of Aquatic Vascular Plants in Wetland of Yellow River Delta, Heilongjiang Agr. Sci., 1, 36–
727 38, 2011. (in Chinese with English abstract)
728 Xue, C.T., Cheng, G.D.: Shelly ridges in west coast of Bohai Sea and Holocene Yellow River Delta system. In: Yang, Z.G.,
729 Lin, H.M. (Eds.), Quaternary Processes and Events in China Offshore and Onshore Areas. China Ocean Press, Beijing,
730 1989. (in Chinese with English abstract)
731 Xue, C.T.: Historical changes in the Yellow River delta, China, Mar. Geol., 113, 321–329, 1993.
732 Xue, C.T., Zhu, X.H., Lin, H.M.: Holocene sedimentary sequence, foraminifera and ostracoda in west coastal lowland of
733 Bohai Sea, China, Quat. Sci. Rev., 14, 521–530, 1995.
734 Yang, Z.S., Ji, Y.J., Bi, N.S., Lei, K., Wang, H.J.: Sediment transport off the Huanghe (Yellow River) delta and in the
735 adjacent Bohai Sea in winter and seasonal comparison, Estuar. Coast. Shelf. S., 93, 173–181, 2011.

https://doi.org/10.5194/cp-2020-20
Preprint. Discussion started: 27 February 2020

Yang, S.X., Li, J., Mao, L.M., Liu, K., Gao, M.S., Ye, S.Y., Yi, S., Zhou, L.Y., Wang, F.F.: Assessing pollen distribution patterns and provenance based on palynological investigation on surface sediments from Laizhou Bay, China: an aid to palaeoecological interpretation, Palaeogeogr. Palaeoclimatol. Palaeoecol., 457, 209–220, 2016.

Yao, Z.Q., Shi, X.F., Li, X.Y., Liu, Y.G., Liu, J., Qiao, S.Q., Bai, Y.Z., Wang, X., Zhu, A.M., Wang, X.C.: Sedimentary environment and paleo-tidal evolution of the eastern Bohai Sea, China since the last glaciation, Quat. Int., 440, 129–138, 2017.

Yi, S., Saito, Y., Oshima, H., Zhou, Y.Q., Wei, H.L.: Holocene environmental history inferred from pollen assemblages in the Huanghe (Yellow River) delta, China: climatic change and human impact, Quat. Sci. Rev., 22, 609–628, 2003.

Zhang, G.S., Wang, R.Q., Song, B.M.: Plant community succession in modern Yellow River Delta, China, J. Zhejiang Univ. Sci., 8(8), 540–548, 2007.

Zhang, X.L., Ye, S.Y., Yin, P., Chen, D.J.: Characters and successions of natural wetland vegetation in Yellow River Delta, Ecol. Env. Sci., 18(1), 292–298, 2009a. (in Chinese with English abstract)

Zhang, X.L., Ye, S.Y., Yin, P., Yuan, H.M.: Flora characteristics of vascular plants of coastal wetlands in Yellow River Delta, Ecol. Env. Sci., 18(2), 600–607, 2009b. (in Chinese with English abstract)

Zhang, Z.H., Leduc, G., Sachs, J.P.: El Niño evolution during the Holocene revealed by a biomarker rain gauge in the Galápagos Islands, Earth Planet. Sci. Lett., 404, 420–434, 2014.

Zhang, P., Hu, R.J., Zhu, L.H., Wang, P., Yin, D.X., Zhang, L.J.: Distributions and contamination assessment of heavy metals in the surface sediments of western Laizhou Bay: Implications for the sources and influencing factors, Mar. Pollut. Bull., https://doi.org/10.1016/j.marpolbul.2017.03.046, 2017.

Zhang, H.X., Zhang, M.L., Xu, T.P., Tang, J.: Numerical Investigations of Tsunami Run-Up and Flow Structure on Coastal Vegetated Beaches, Water, https://doi.org/10.3390/w10121776, 2018.

Zhao, C., Liu, Z.H., Rohling, E.J., Yu, Z.C., Liu, W.G., He, Y.X., Zhao, Y., Chen, F.H.: Holocene temperature fluctuations in the northern Tibetan Plateau, Quat. Res., 80, 55–65, 2013.

Zheng, Z., Yang, S.X., Deng, Y., Huang, K.Y., Wei, J.H., Berne, S., Suc, J.P.: Pollen record of the past 60 ka BP in the Middle Okinawa Trough: Terrestrial provenance and reconstruction of the paleoenvironment, Palaeogeogr. Palaeoclimatol. Palaeoecol., 307, 285–300, 2011.

Zhou, L.Y., Liu, J., Saito, Y., Gao, M.S., Diao, S.B., Qiu, J.D., Pei, S.F.: Modern sediment characteristics and accumulation rates from the delta front to prodelta of the Yellow River (Huanghe), Geo-Mar. Lett., 36, 247–258, 2016.

Zhou, Z., Bian, C., Wang, C., Jiang, W., Bi, R.: Quantitative assessment on multiple timescale features and dynamics of sea surface suspended sediment concentration using remote sensing data, J. Geophys. Res-Oceans., 122, 8739–8752, 2017.

https://doi.org/10.5194/cp-2020-20
Preprint. Discussion started: 27 February 2020

Climate of the Past Discussions

771 **Table captions**

772

773 **Table 1:** AMS radiocarbon dates from core CJ06-435 and one tie points corresponding to the deepest onset of ^{137}Cs in
774 environmental samples at measurable levels; for calibration in years before present (a BP) 0 = 1950 AD.

775

776

777

Core depth (cm)	Materials	Radiocarbon date (a)	Age error (a)	Calibrated age (1σ) (a BP)	Mean calibrated age (a BP)	Laboratory
25	^{137}Cs	–	–	–	–4	NIGLAS
7	Mixed foraminifera	3020	30	2854-3039	2951	Beta
13	Mixed foraminifera	2990	30	2817-2997	2913	Beta
17	Mixed foraminifera	3060	30	2908-3102	3003	WHOI
59	Mixed foraminifera	3340	30	3270-3485	3359	Beta
69	Mixed foraminifera	3590	25	3563-3725	3656	WHOI
87	Mixed foraminifera	4450	30	4695-4878	4801	Beta
119	Mixed foraminifera	5200	30	4812-4965	5706	WHOI
129	Mixed foraminifera	4520	30	4812-4965	4894	Beta
161	Mixed foraminifera	6020	30	6501-6667	6592	WHOI
183	Mixed foraminifera	6340	35	6886-7081	6981	WHOI

778 **Table 1**

779 AMS radiocarbon dates from core CJ06-435 and one tie points corresponding to the deepest onset of ^{137}Cs in environmental
780 samples at measurable levels; for calibration in years before present (a BP) 0 = 1950 AD.

781

782

783

784

785

786

787

788

https://doi.org/10.5194/cp-2020-20
Preprint. Discussion started: 27 February 2020


Climate of the Past Discussions

Figure caption

Figure 1: (a) Locations of core CJ06-435 (red circle) and other sites referred to in this study (blue circles): ① Bayanchagan Lake (Jiang et al., 2006), ② Guliya ice core (Thompson et al., 1997), ③ Sahara sand wetland (Rao et al., 2019), ④ Narenxia Peat (Feng et al., 2017). (b) Topography and circulation of the study area. Circulation pattern (modified from Yao et al., 2017) is indicated by the black (winter), red (summer) and green (both summer and winter) arrows. YSWC: Yellow Sea Warm Current; LCC: Liaonan Coastal Current; BSCC: Bohai Sea Coastal Current.

Figure 2: Lithology, grain size, color reflectance *L** and *a**, magnetic susceptibility, and activity profiles for ^{137}Cs and ^{210}Pb of core CJ06-435.

Figure 3: Percentage diagram of the principal pollen taxa from core CJ06-435. Pollen zonation is based on CONISS results.

Figure 4: Concentration diagram of the principal pollen taxa from core CJ06-435.

Figure 5: Spatial distribution of modern pollen percentage (black solid circle, %) and concentration (red open circle, grains/g) in Laizhou Bay, Bohai Sea (modified from Yang et al., 2016).

Figure 6: (a-f) Vertical profiles of grain-size parameters and halophytic and xerophytic herb (Chenopodiaceae and *Artemisia*) pollen percentage and concentration of core CJ06-435 (Mz – mean grain size). (g) The location of Yellow River superlobe 1 (Lijin superlobe) and superlobe 10 (Modern superlobe) (modified after Xue, 1993).

Figure 7: (a) Correlating proxy to paleo-superlobe variation of the YR, from top to bottom: percentage of Cyperaceae, Chenopodiaceae, and *Artemisia* pollen; concentration of Chenopodiaceae, *Artemisia*, and Cyperaceae pollen; sand percentage. (b) Detailed pollen and grain size profiles representing salt marsh species (Cyperaceae, Chenopodiaceae, *Artemisia*) relative abundances and hydrodynamic change during the formation of Yellow River superlobe 1 and 10. Pollen percentage of Cyperaceae, Chenopodiaceae and *Artemisia* from core CJ06-435 indicating the directional alternation of salt marshes along the Bohai Sea, ①— Unchannelized river flow characterized the onset of Yellow River channel shift, caused a large amount of river–derived sediment accumulation in the floodplain and destroyed the sedges in the coastal depression; ②—Along with the formation of a new channel, lateral migration of the lower

https://doi.org/10.5194/cp-2020-20
Preprint. Discussion started: 27 February 2020

Climate of the Past Discussions

channel stopped, and new intertidal mudflat was formed. Pioneer species (Chenopodiaceae, *Artemisia*) first colonize bare zones of lower and middle marsh areas.

Figure 8: Comparison of relevant Holocene temperature records (locations of the sites where the records are derived are illustrated in Fig. 1a) with solar irradiance and ENSO proxy records derived from the eastern equatorial Pacific. (a) Summer (mean of June) insolation irradiance for the Northern Hemisphere (40°N). (b) *Quercus* pollen percentage record from core CJ06-435, bold-red line is the five-point running average. (c) Pollen-based mean annual temperature (MAT) record from Narenxia Peat in the southern Altai (Feng et al., 2017). (d) $\delta^{18}O$ record from the Guliya ice core in the western Kunlun Shan (Thompson et al., 1997). (e) Alpine peat α-cellulose $\delta^{13}C$ record from the Altai Mountains in central Asia (Rao et al., 2019). (f) Pollen-based mean annual temperature record from Lake Bayanchagan in Inner Mongolia, North China (Jiang et al., 2006). (g) Botryococcene concentrations in the El Junco sediment, a proxy for frequency of El Niño events (Zhang et al., 2014). (h) Variance of $\delta^{18}O$ values of individual planktonic foraminifera (*G. ruber*) in sediment core V21–30 from the Galápagos region, a proxy for ENSO variance (Koutavas and Joanides, 2012).

https://doi.org/10.5194/cp-2020-20
Preprint. Discussion started: 27 February 2020

Climate of the Past
Discussions
Open Access
EGU

Figure 1

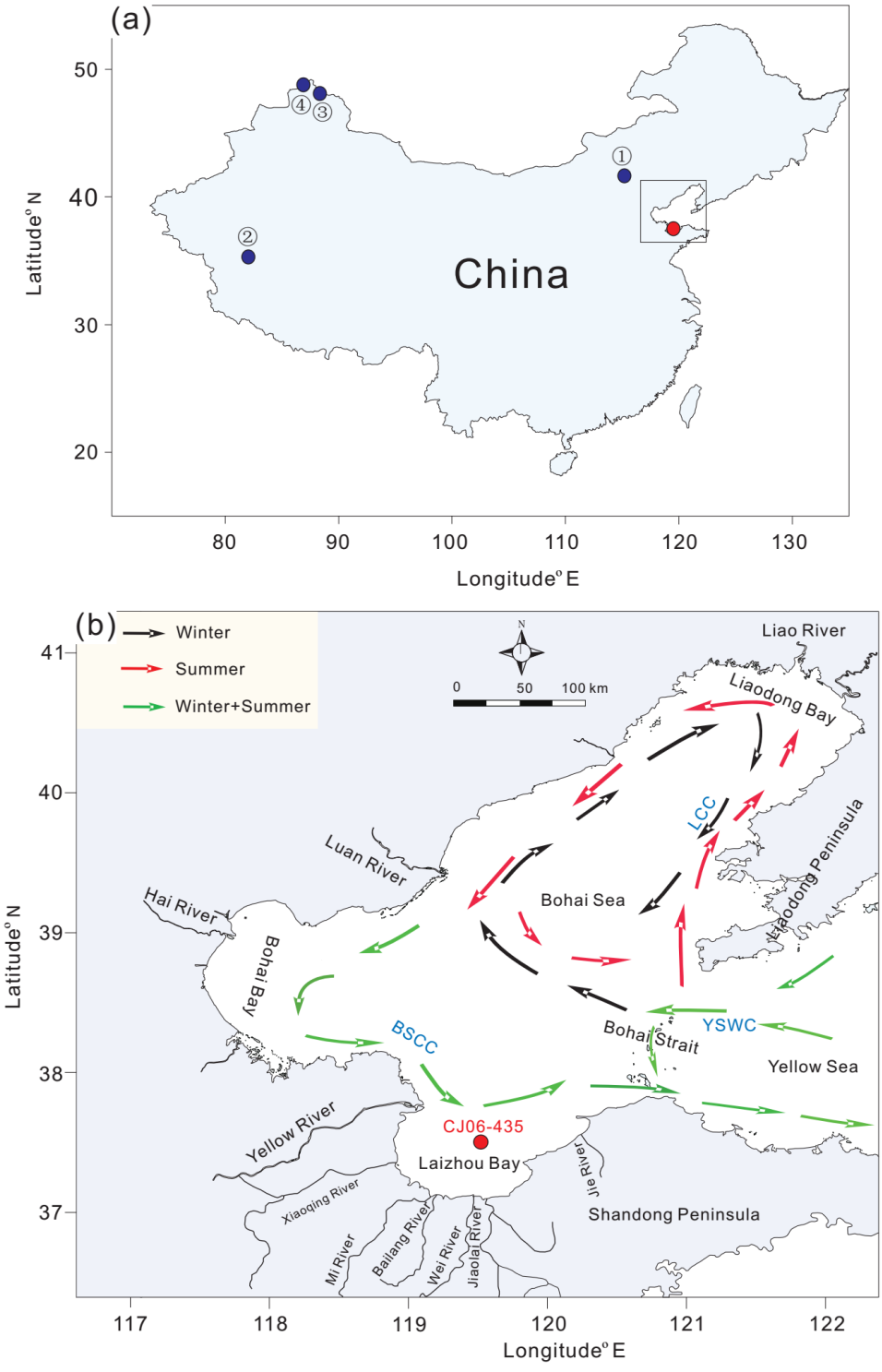

856

https://doi.org/10.5194/cp-2020-20
Preprint. Discussion started: 27 February 2020

Climate of the Past Discussions
Open Access
EGU

Figure 2

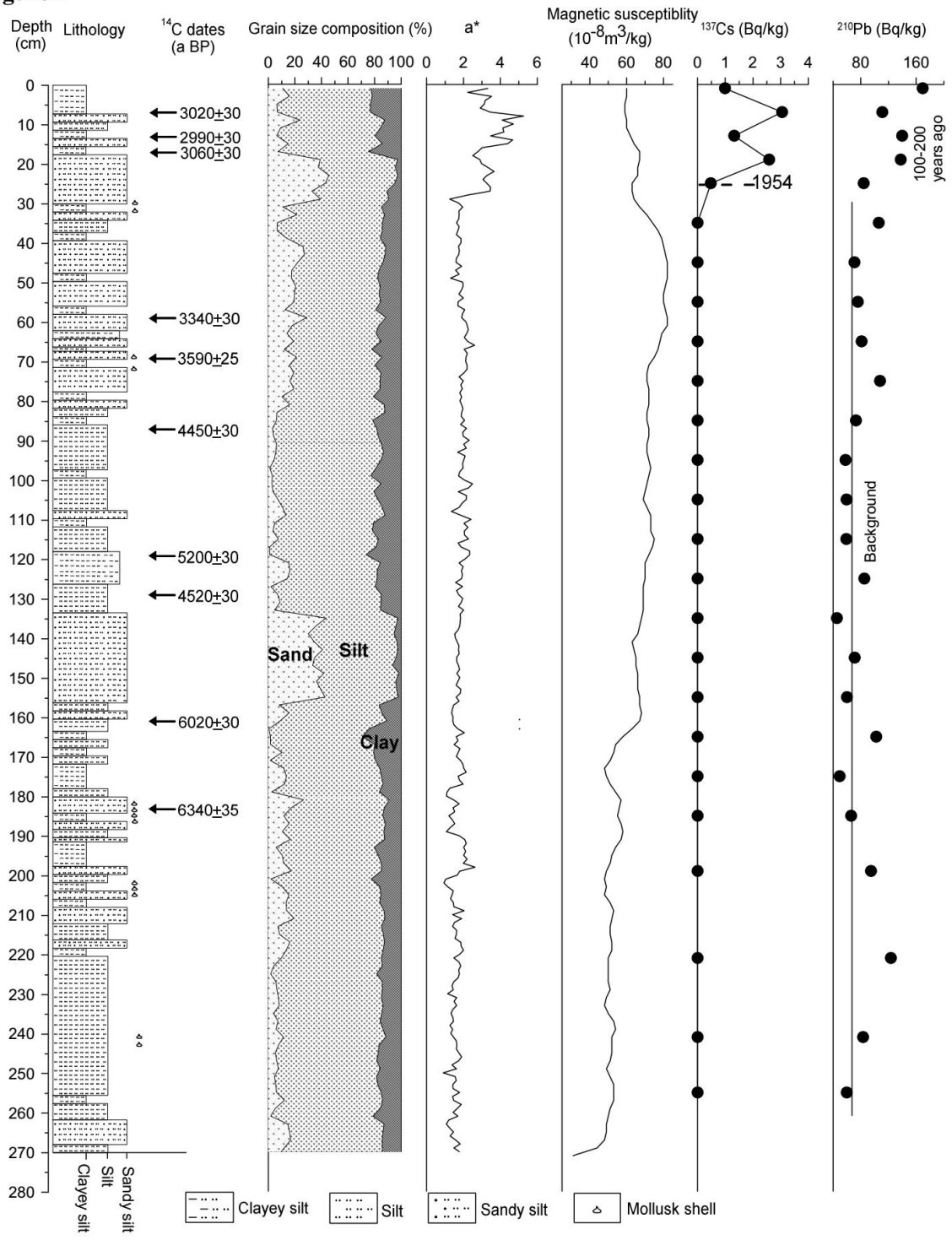

857

https://doi.org/10.5194/cp-2020-20
Preprint. Discussion started: 27 February 2020

Climate of the Past
Discussions
Open Access
EGU

Figure 3

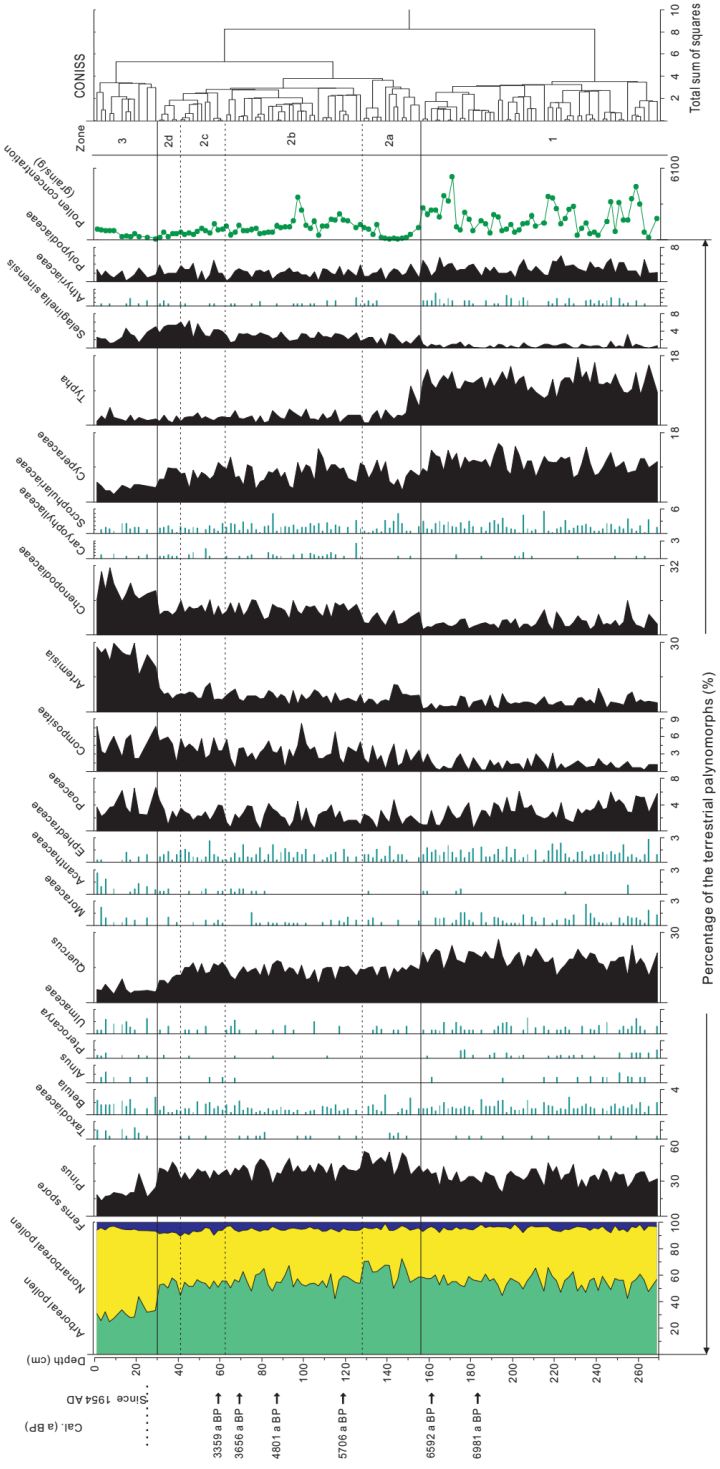

https://doi.org/10.5194/cp-2020-20
Preprint. Discussion started: 27 February 2020

Climate of the Past Discussions
Open Access
EGU

Figure 4

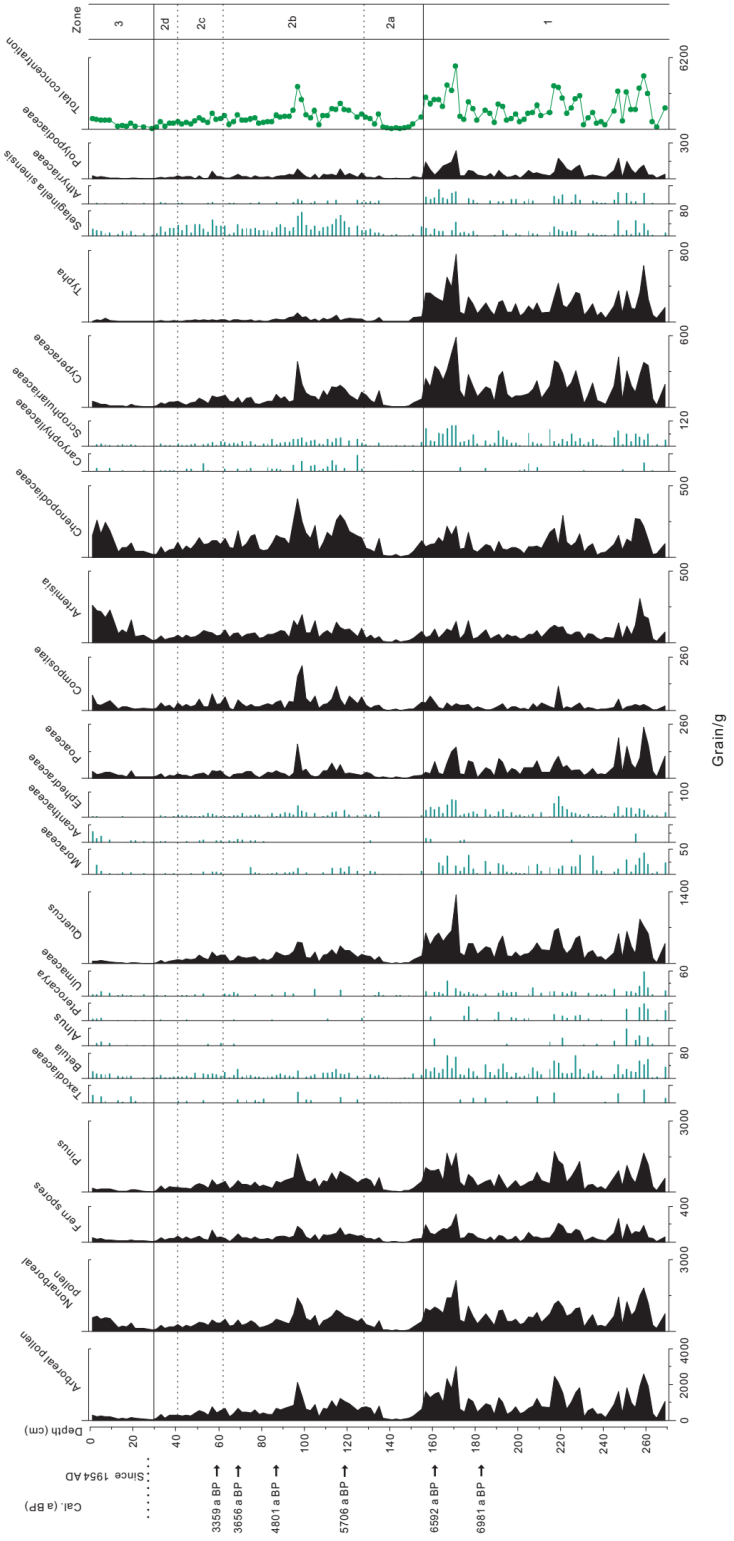

https://doi.org/10.5194/cp-2020-20
Preprint. Discussion started: 27 February 2020

Climate of the Past Discussions
Open Access
EGU

Figure 5

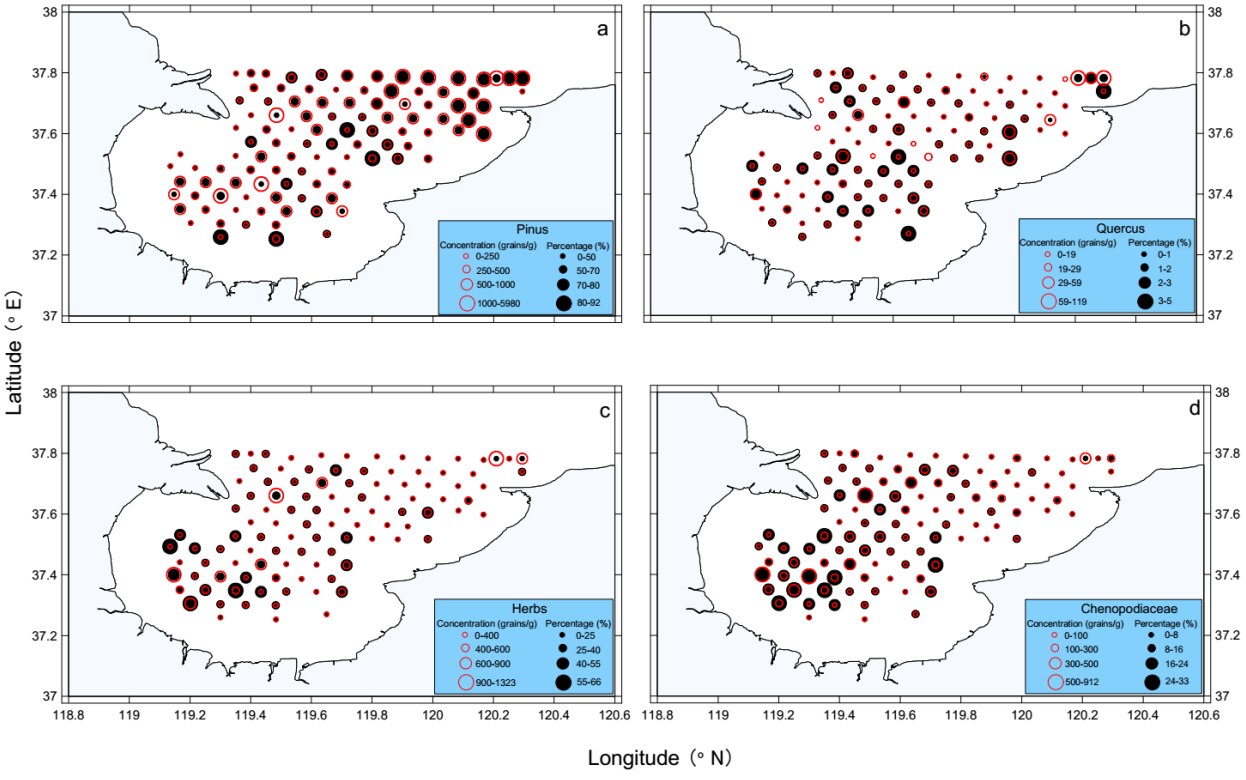

https://doi.org/10.5194/cp-2020-20
Preprint. Discussion started: 27 February 2020

Climate of the Past Discussions
Open Access
EGU

Figure 6

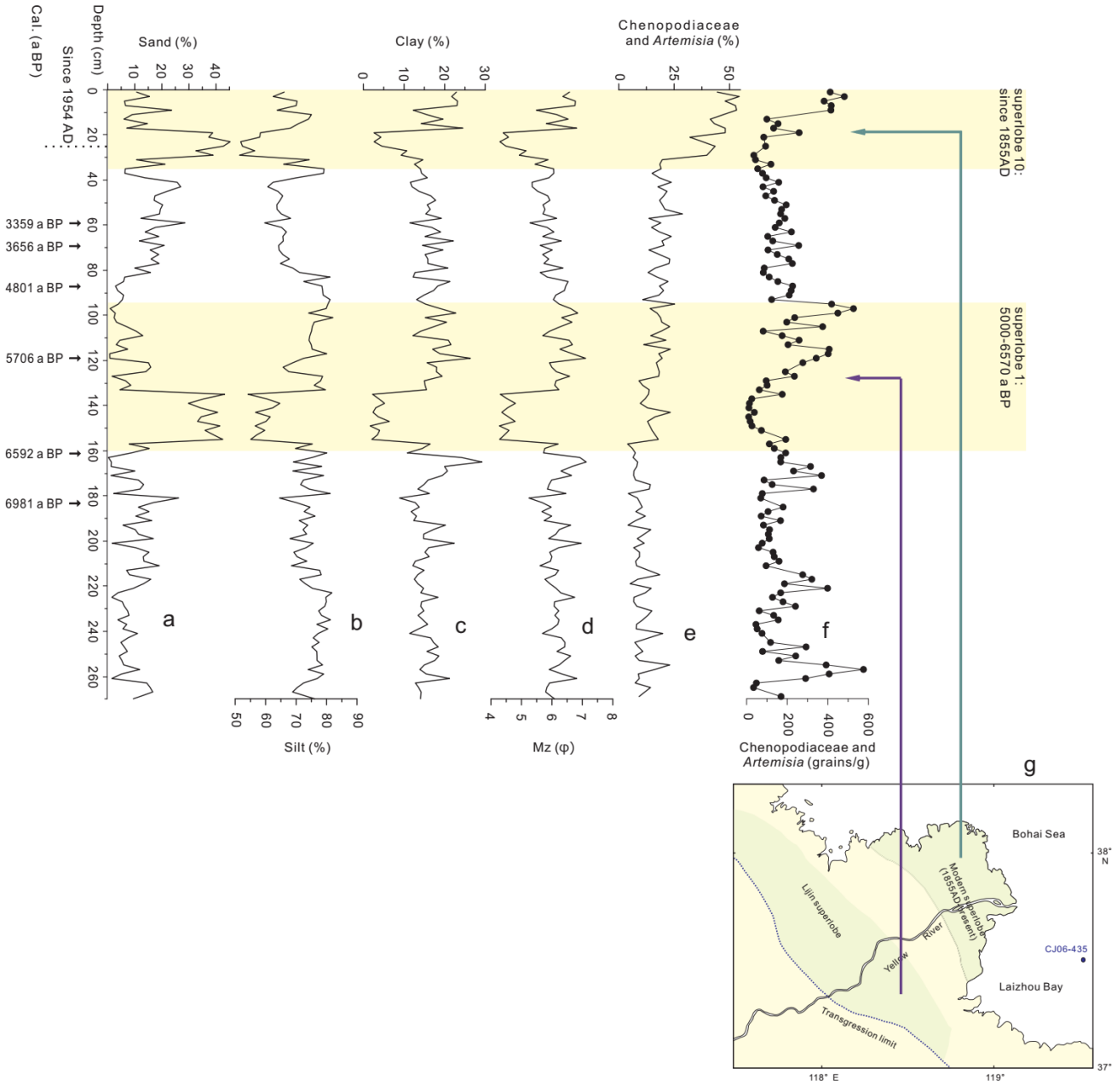

https://doi.org/10.5194/cp-2020-20
Preprint. Discussion started: 27 February 2020

Climate of the Past Discussions

Figure 7

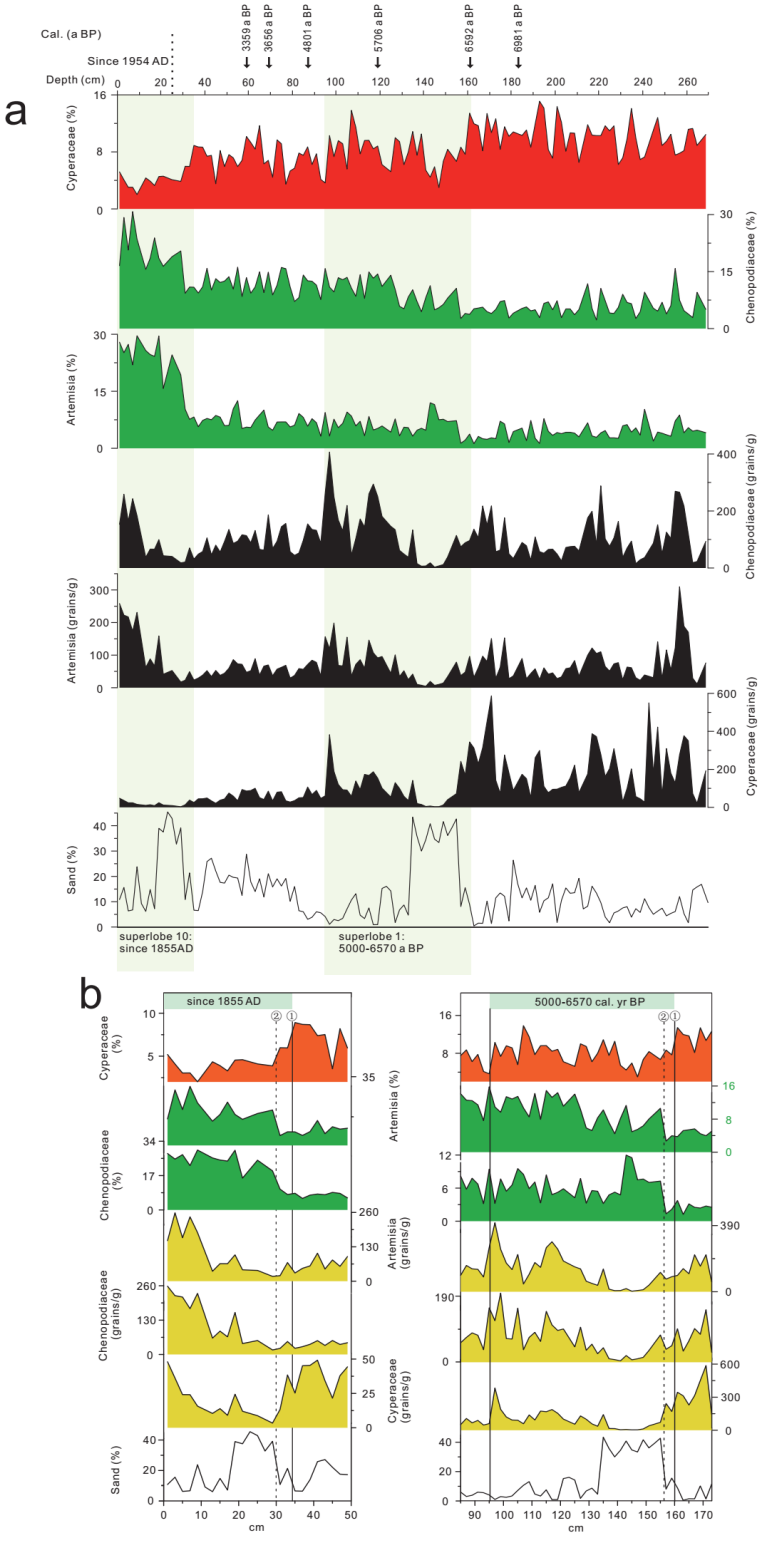

https://doi.org/10.5194/cp-2020-20
Preprint. Discussion started: 27 February 2020

Climate of the Past Discussions
Open Access
EGU

Figure 8

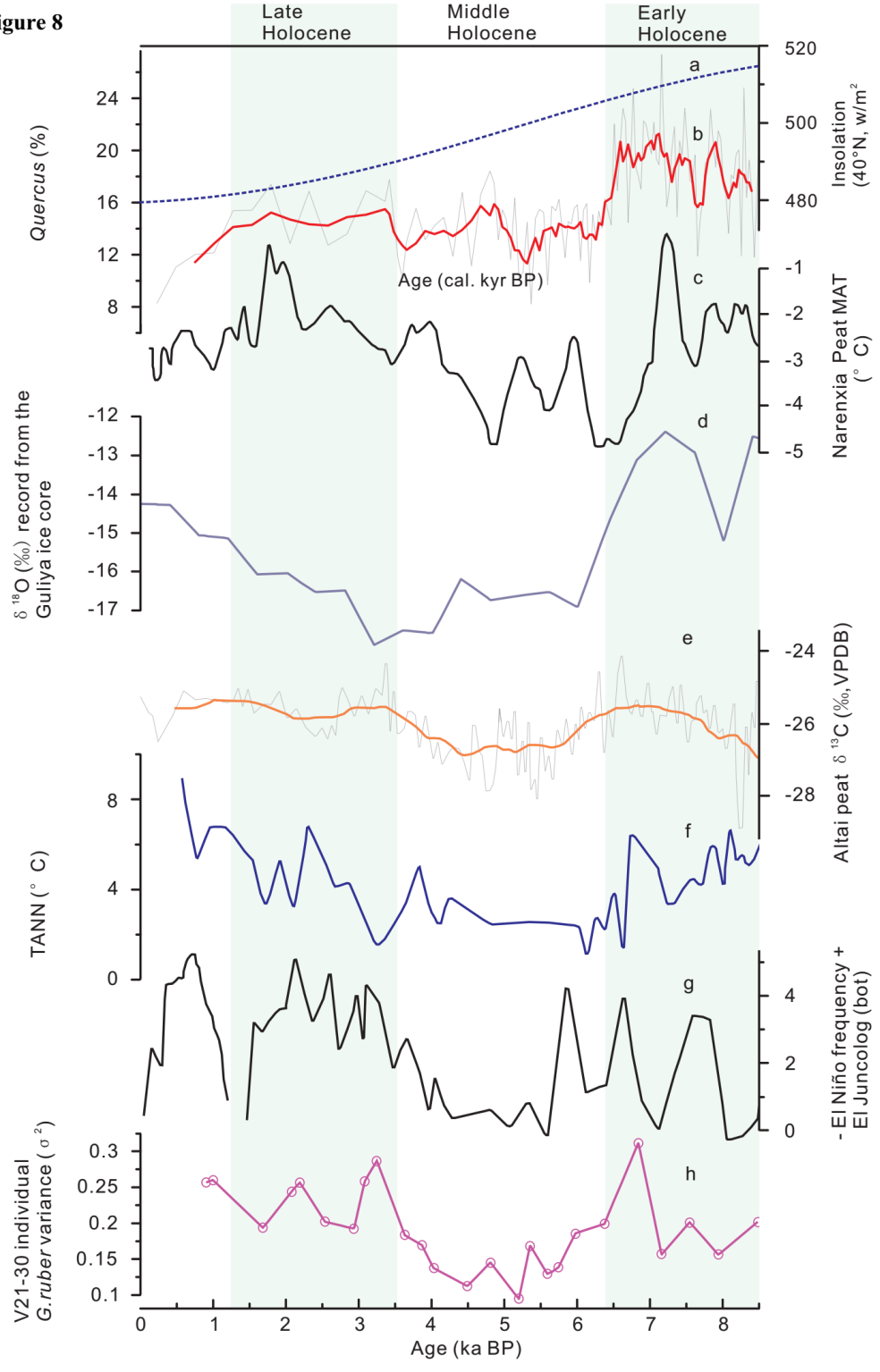

873